Soil Dynamics and Earthquake Engineering 39 (2012) 61–77

Contents lists available at SciVerse ScienceDirect

Soil Dynamics and Earthquake Engineering

journal homepage: www.elsevier.com/locate/soildyn

The exact and approximate conditional spectra in the multi-seismic-sources regions

Hossein Ebrahimian [a], Alireza Azarbakht [b,*], Armin Tabandeh [a], Ali Akbar Golafshani [a]

[a] Department of Civil and Environmental Engineering, Sharif University of Technology, Tehran, Iran
[b] Department of Civil Engineering, Faculty of Engineering, Arak University, Arak, 38156-8-8349, Iran

ARTICLE INFO

Article history:
Received 29 October 2011
Received in revised form
27 January 2012
Accepted 11 March 2012
Available online 31 March 2012

Keywords:
Selection of ground motion records
Nonlinear dynamic analysis
Conditional spectrum
Probabilistic seismic hazard deaggregation
Persian Gulf region

ABSTRACT

The exact and two approximate conditional spectra are compared in this manuscript as a target spectrum for the purpose of ground motion selection. The considered site is a real offshore site located at South Pars Gas Field in the Persian Gulf region. This case study site is influenced by four major seismic area sources in which the deaggregation results confirm that many comparable seismic scenarios can be taken into account. Therefore, an alternative to the conventional approximate conditional spectrum is proposed that has a small deviation from the exact solution. In addition, the use of different conditioning status of the probabilistic seismic hazard deaggregation (i.e., occurrence versus exceedance of the target spectral acceleration) for calculating the exact distribution of conditional spectrum was investigated. The results show that one of the proposed approximate approaches leads to conditional distributions which provide acceptable agreement with those obtained from the exact solution.

1. Introduction

Nonlinear dynamic analyses of structures are becoming increasingly prevalent in codes and regulatory documents with the aim of increasing the accuracy of the structural response estimation. This is in line with the developments in capability of the technical software for carrying out nonlinear dynamic analysis. For conducting response history analysis, most of the current building codes enforce the requirements to match the characteristics of the event and the site as well as ensuring that the mean spectrum of the selected records matches to the target Uniform Hazard Spectrum (UHS) in the recommended period interval (e.g., [1–4]). However, the spectral values of UHS at different period-ranges come from dissimilar causal events; hence, it is unlikely for an individual record to have spectral accelerations as high as the UHS throughout the considered period-range. As a result, the exceedance of all spectral values of UHS simultaneously has much lower rate and UHS results in an unjustifiably conservative scenario of earthquakes occurring due to different seismic sources acting all together [5–9]. Recognizing that the resulted structural response, associated with UHS-based record selection, is quite conservative, less biased estimates of response can be obtained by utilizing a target spectrum named Conditional Mean Spectrum (CMS) [7–9] in the probabilistic seismic assessment of structures. The CMS employs the advantages of the epsilon, ε, which is a ground motion characteristic that affects the structural response. The CMS-based record selection accounts successfully for the effect of ε without using a vector-valued intensity measure (IM) consisting the spectral acceleration at the period of interest, $Sa(T^*)$, and ε [7,10]. Furthermore, a new spectral shape indicator, named Eta, has been recently introduced by Mousavi et al. [11] which is able to better capture the correlation between the structural response and the spectral shape than the convenient epsilon. It can be implemented for the purpose of the current study in a separate research, as well.

The probabilistic seismic hazard analysis (PSHA) deaggregation of magnitude, distance and ε associated with a given $Sa(T^*)$ level [12] can be used to determine the conditional mean and variance of a response spectrum associated with a given $Sa(T^*)$ level. The ground motion records can be subsequently selected such that their scaled response spectra to $Sa(T^*)$ match this conditional spectrum, without further considering the magnitude, distance or ε values of those records [13–15]. The CMS-based record selection can widen the range of the alternative records for the nonlinear dynamic analysis since the selected ground motions should no longer match the triplet (M, R,ε) explicitly, i.e., they possess only a spectral shape that matches the target spectrum with the causal event.

* Corresponding author. Tel.: +98 861 417 3446.
E-mail address: a-azarbakht@araku.ac.ir (A. Azarbakht).

0267-7261/$ - see front matter © 2012 Elsevier Ltd. All rights reserved.
http://dx.doi.org/10.1016/j.soildyn.2012.03.004

Baker and Cornell [7] discussed about the exact and approximate distributions of the conditional spectrum (CS). It is worth stating at this point that the CS abbreviation in the current manuscript stands for the mean and distribution of the conditional spectra while the CMS refers to the median of this distribution. The exact distribution of the CS utilizes the multiple causal magnitudes and distances from a given seismic hazard deaggregation associated with the prescribed $Sa(T^*)$ level. However, Baker and Cornell [7] concluded that using the mean values for magnitude, distance and epsilon (denoted by $\overline{M}$, $\overline{R}$ and $\overline{\varepsilon}$), directly obtained from the seismic hazard deaggregation, can lead to the approximate estimates of the CS which is comparable with the exact distribution. Moreover, they provided their concluding remarks based upon a hypothetical site with a relatively simple source model. As a result, the issue of the common CS's approximation needs to be further explored in practice especially when the hazard of the site is influenced by multiple seismic sources with dissimilar source characteristics. The purpose of the current research is to further study the refinements to the CS's approximations through a specific site by means of finding the most efficient approximate approach, which has a small deviation from the exact solution. A real case-study has been considered in this paper which is an offshore site in the South Pars Gas Field located in Persian Gulf region in southern coast of Iran. The goal of imposing refinements to the CS's computations can facilitate the hazard-consistent ground motion selection to implement in the probabilistic assessment of offshore facilities. Furthermore, the probabilistic seismic hazard estimation for the considered site is intended to be at the bedrock elevation; therefore, the selected hazard-consistent ground motions are representative of those observed on rock outcrop which can be used as bedrock-level records for estimation of the free-field motions [16,17]. In addition, this manuscript provides further insights to study the effect of implementing different definitions of deaggregation [12,18] on the exact distribution of the CS.

2. Selected intensity measures for the purpose of conditioning

Since the fundamental aspects of the employed exact and approximate CS are described in the following sections, this section aims to summarize the IMs utilized in this study for the purpose of conditioning. The goal of the probabilistic assessment benefits greatly from having a direct link to the ground-motion hazard as the rate of exceedance of the associated $Sa(T^*)$ value. Therefore the CS conditioned on the target Sa value at a specific period, T^*, is desirable. However, the structural response of offshore facilities in the considered site is sensitive to multiple Sa values at multiple periods. Hence, the conditioning status in the current research is the IM which was originally proposed by Baker and Cornell [7,8]. This IM averages Sa values over a range of periods, and it is denoted herein as $Sa_{\mathrm{avg}}(\mathbf{T}^*)$, where $\mathbf{T}^*$ is the vector of n periods of interest, $\langle T^{(1)},\ldots,T^{(n)}\rangle$. The average spectral acceleration is actually the geometric mean of the spectral acceleration values at a set of periods:

$$Sa_{\mathrm{avg}}(\mathbf{T}^*) = Sa_{\mathrm{avg}}(T^{(1)},\ldots,T^{(n)}) = \left(\prod_{i=1}^{n} Sa(T^{(i)})\right)^{1/n} \tag{1}$$

The purpose of using geometric mean in Eq. (1) is due to the fact that while $\ln Sa(T^{(i)})$ terms have a joint normal distribution, the expression for $\ln Sa_{\mathrm{avg}}(\mathbf{T}^*)$ is normally distributed as well. The ground motion hazard for $Sa_{\mathrm{avg}}(\mathbf{T}^*)$ can be easily developed based on existing ground motion prediction models for convenient spectral acceleration values and the correlation information between the spectral values at different periods (for more details see [7,8,19]). Bianchini et al. [20] recommended Sa_{avg} to be calculated at ten discrete points logarithmically spaced. This is for the reason that the logarithmic-spacing approach samples more points in the range of short periods, where the spectrum has a jagged shape, in comparison with the arithmetic-spacing approach.

For the considered site in this research, the fundamental period of the existing complex offshore systems was estimated to be around 1.5 to 2 s. Moreover, it was found that the periods of offshore systems range from 0.5 to 4 s considering the higher-modes and the nonlinear response effects [21,22]. As a result, for consideration of the higher modes effects and/or the nonlinearity in the response of the complex offshore platform, four different IMs, as illustrated in Table 1, were implemented for the conditioning status of the CS in the subsequent sections.

3. The exact conditional spectra

In general, a variety of M and R values contribute to the $Sa_{\mathrm{avg}}(\mathbf{T}^*)$ hazard level of interest. The variability in the causal M, R and ε values alters theoretically the CS predictions. The mean and variance of $\ln Sa(T)$ at all periods conditioned on $\ln Sa(T^*) = x$ has been derived [[7], Appendix E] by employing the concept of the Bayesian (or Compound) distribution [23]. Consequently, in the case of the current study, the exact mean and variance of CS at a specific period, T, conditioned on target $\ln Sa_{\mathrm{avg}}(\mathbf{T}^*) = x$, which are denoted by $\ln Sa_{\mathrm{CMS}}^{\mathrm{exact}}(T)$ and $\sigma^2_{\ln Sa_{\mathrm{CMS}}^{\mathrm{exact}}(T)}$, can be expressed as written in Eqs. (2) and (3).

$$\begin{aligned}\ln Sa_{\mathrm{CMS}}^{\mathrm{exact}}(T) = \mu^{\mathrm{exact}}_{\ln Sa(T)|\ln Sa_{\mathrm{avg}}(\mathbf{T}^*)=x} &= \sum_{n=1}^{N_S} p_n \\ &\times \left(\sum_{k=1}^{N_M}\sum_{j=1}^{N_R} p_{jk}[\mu_{\ln Sa(T)}(m_k,r_j,\varphi_n) + \rho(T,\mathbf{T}^*)\cdot\varepsilon_{LB}\cdot\sigma_{\ln Sa(T)}]\right) \\ &= \sum_{n=1}^{N_S} p_n \cdot \left(\sum_{k=1}^{N_M}\sum_{j=1}^{N_R} p_{jk}[\mu_{\ln Sa(T)|\ln Sa_{\mathrm{avg}}(\mathbf{T}^*)=x}(m_k,r_j,\varphi_n)]\right) \\ &= \sum_{n=1}^{N_S} p_n \cdot \mu_{\ln Sa(T)\ln Sa_{\mathrm{avg}}(\mathbf{T}^*)=x,n}\end{aligned} \tag{2}$$

$$\sigma^2_{\ln Sa_{\mathrm{CMS}}^{\mathrm{exact}}(T)} = (\sigma^{\mathrm{exact}}_{\ln Sa(T)|\ln Sa_{\mathrm{avg}}(\mathbf{T}^*)=x})^2 = (1-\rho^2(T,\mathbf{T}^*))$$

Table 1
Four different IMs employed in current study.

IM	General description	n[a]
(1) Sa_{avg}(0.5 s,… ,4 s)	Considering the issues of the period elongation and the higher-modes simultaneously	20
(2) Sa_{avg}(0.5 s,… ,2 s)	Taking into account only the higher-modes of vibration	14
(3) Sa_{avg}(1.5 s,… ,4 s)	Taking into account only the elongation of the first-mode period	10
(4) Sa(2 s)	Considering only the natural period of the system	—

[a] Number of logarithmically spaced period-points.

$$\times \sum_{n=1}^{N_S} p_n \times \left(\sum_{k=1}^{N_M} \sum_{j=1}^{N_R} p_{jk} \cdot \sigma^2_{\ln Sa(T)} \right) + \sum_{n=1}^{N_S} p_n \times \left(\sum_{k=1}^{N_M} \sum_{j=1}^{N_R} p_{jkn} \cdot [\mu_{\ln Sa(T)|\ln Sa_{\text{avg}}(\mathbf{T}^*)=x}(m_k,r_j,\varphi_n) - \mu_{\ln Sa(T)|\ln Sa_{\text{avg}}(\mathbf{T}^*)=x,n}]^2 \right) \quad (3)$$

where N_S denotes the number of seismic sources at the prescribed site; N_M and N_R indicate the number of magnitude, m, and distance, r, segments within each seismic source respectively; $\mu_{\ln Sa(T)}(m_k,r_j,\varphi_n)$ and $\sigma_{\ln Sa(T)}$ are the predicted mean and standard deviation of $\ln Sa(T)$, which are specified by a standard ground motion prediction model (i.e., Campbell and Bozorgnia [24] NGA attenuation relationship (CB08) in this study), for a scenario of magnitude, m_k, distance, r_j, and other site-source parameters denoted by φ_n. The parameter,φ_n, refers to local site condition, basin effect and faulting mechanism, associated with the nth seismic source. It is worth noting that according to the CB08 relationship, the predicted standard deviation on the reference rock is only a function of the respective period, T. However Eq. (3) in this section is arranged for the general conditions where $\sigma_{\ln Sa(T)}$ is generally a function of the respective scenario event. Moreover, the parameter ε_{LB}, as written in Eq. (4), denotes the lower-bound epsilon associated with the occurrence of $Sa_{\text{avg}}(\mathbf{T}^*)$ based on each individual causal event within different seismic sources, which is consistent with the treatment of ε by McGuire [12].

$$\varepsilon_{LB} = \varepsilon \,|\, (\ln Sa_{\text{avg}}(\mathbf{T}^*) = x, M = m_k, R = r_j, \text{event}_n) = \frac{x - \mu_{\ln Sa_{\text{avg}}(\mathbf{T}^*)}(m_k,r_j,\varphi_n)}{\sigma_{\ln Sa_{\text{avg}}(\mathbf{T}^*)}} \quad (4)$$

In Eq. (4), $\mu_{\ln Sa_{\text{avg}}(\mathbf{T}^*)}$ and $\sigma_{\ln Sa_{\text{avg}}(\mathbf{T}^*)}$ are the predicted mean and standard deviation of $\ln Sa_{\text{avg}}(\mathbf{T}^*)$, respectively, which can be expressed as: (see also [8,19]):

$$\mu_{\ln Sa_{\text{avg}}(\mathbf{T}^*)} = \frac{1}{n} \sum_{i=1}^{n} \mu_{\ln Sa(T^{(i)})}(m,r,\varphi) \quad (5)$$

$$\sigma_{\ln Sa_{\text{avg}}(\mathbf{T}^*)} = \frac{1}{n} \sqrt{\sum_{i=1}^{n} \sum_{j=1}^{n} \rho(T^{(i)},T^{(j)}) \cdot \sigma_{\ln Sa(T^{(i)})} \cdot \sigma_{\ln Sa(T^{(j)})}} \quad (6)$$

where $\rho(T^{(i)},T^{(j)})$ is the correlation coefficient between spectral accelerations at two observed periods. The correlation model, proposed by Baker and Jayaram [19], is utilized in this study which is valid over a wide period range of 0.01 to 10 s. Moreover, $\rho(T,\mathbf{T}^*)$ in Eq. (2) is the correlation coefficient between $\ln Sa(T)$ and $\ln Sa_{\text{avg}}(\mathbf{T}^*)$, and can be computed as (see also [8]):

$$\rho(T,\mathbf{T}^*) = \frac{\text{Cov}[\ln Sa(T), \ln Sa_{\text{avg}}(\mathbf{T}^*)]}{\sigma_{\ln Sa(T)} \cdot \sigma_{\ln Sa_{\text{avg}}(\mathbf{T}^*)}} = \frac{(1/n) \sum_{i=1}^{n} \text{Cov}[\ln Sa(T), \ln Sa(T^{(i)})]}{\sigma_{\ln Sa(T)} \cdot \sigma_{\ln Sa_{\text{avg}}(\mathbf{T}^*)}} \quad (7)$$

According to Eq. (6), $\rho(T,\mathbf{T}^*)$ can be expressed as:

$$\rho(T,\mathbf{T}^*) = \frac{\sum_{i=1}^{n} \rho(T,T^{(i)}) \cdot \sigma_{\ln Sa(T^{(i)})}}{\sqrt{\sum_{i=1}^{n} \sum_{j=1}^{n} \rho(T^{(i)},T^{(j)}) \cdot \sigma_{\ln Sa(T^{(i)})} \cdot \sigma_{\ln Sa(T^{(j)})}}} \quad (8)$$

Again, $\rho(T,T^{(i)})$ is the correlation coefficient between two observed periods, T and $T^{(i)}$. If the vector $\mathbf{T}^*$ has only a particular element equal to $T^{(k)}$, one can observe that the predicted correlation coefficient in Eq. (8) becomes $\rho(T,T^{(k)})$. Similarly the predicted $\mu_{\ln Sa_{\text{avg}}(\mathbf{T}^*)}$ and $\sigma_{\ln Sa_{\text{avg}}(\mathbf{T}^*)}$ are $\mu_{\ln Sa(T^{(k)})}$ and $\sigma_{\ln Sa(T^{(k)})}$ in this case. In addition, $\mu_{\ln Sa(T)|\ln Sa_{\text{avg}}(\mathbf{T}^*)=x}(m,r,\varphi_n)$ in Eqs. (2) and (3) is defined as the CMS for the scenario event of $M=m$ and $R=r$, given the particular source n; consequently, $\mu_{\ln Sa(T)|\ln Sa_{\text{avg}}(\mathbf{T}^*)=x,n}$ indicates the CMS associated with the seismic source n. Finally, p_{jk} indicates the probability of each possible (M,R) combination within each seismic source, n, causing the target $Sa_{\text{avg}}(\mathbf{T}^*)=y$ ($\ln y = x$), which can be estimated by using different approaches of seismic hazard deaggregation; and p_n is the probability associated with each seismic source n.

Generally, two different definitions for deaggregation have been proposed. Bazzurro and Cornell [18] definition provides the distribution of M, R and ε given that $Sa_{\text{avg}}(\mathbf{T}^*) > y$. Thus, the probability term p_{jk} can be expressed as:

$$p_{jk} = \frac{\sum_{\varepsilon} v_n \cdot H_{\varepsilon_{LB}}(\varepsilon) \cdot \phi(\varepsilon) \Delta\varepsilon \cdot P[R=r_j] \cdot P[M=m_k]}{\lambda_{Sa_{\text{avg}}(\mathbf{T}^*)>y,n}} \quad (9)$$

where v_n represents the annual rate of occurrence of the nth seismic source or the rate of seismicity for the nth seismic source; $H_{\varepsilon_{\text{LB}}}(\varepsilon)$ is the Heaviside step function at $\varepsilon=\varepsilon_{\text{LB}}$; $\phi(\bullet)$ is the standardized Gaussian Probability Density Function (PDF); $\Delta\varepsilon$ is the differential of the epsilon distribution; the expressions $P[R=r]$ and $P[M=m]$ are the likelihood that the site-to-source distance and magnitude equal to the specified values r and m, respectively; and finally $\lambda_{Sa_{\text{avg}}(\mathbf{T}^*)>y,n}$ is the hazard in terms of the mean annual rate of exceedance of $Sa_{\text{avg}}(\mathbf{T}^*)$ from a given level, y, associated with the nth seismic source. Moreover, $p_n = (\lambda_{Sa_{\text{avg}}(\mathbf{T}^*)>y,n} / \lambda_{Sa_{\text{avg}}(\mathbf{T}^*)>y})$ where the total hazard $\lambda_{Sa_{\text{avg}}(\mathbf{T}^*)>y}$ equals to:

$$\lambda_{Sa_{\text{avg}}(\mathbf{T}^*)>y} = \sum_{n=1}^{N_S} \sum_{k=1}^{N_M} \sum_{j=1}^{N_R} \sum_{\varepsilon} v_n \cdot H_{\varepsilon_{LB}}(\varepsilon) \cdot \phi(\varepsilon) \Delta\varepsilon \cdot P[R=r_j] \cdot P[M=m_k] \quad (10)$$

On the other hand, the definition of the deaggregation which was proposed by McGuire [12] provides the distribution of M, R and ε given $Sa_{\text{avg}}(\mathbf{T}^*)=y$. In order to derive an analytical expression for p_{jk} in this case, one should estimate the hazard in terms of the mean annual rate of $Sa_{\text{avg}}(\mathbf{T}^*)$ to be equal to a given value y (i.e., $\lambda_{Sa_{\text{avg}}(\mathbf{T}^*)=y}$). This term can be estimated directly by using Eq. (10), in which the Heaviside step function, $H_{\varepsilon_{\text{LB}}}(\varepsilon)$, is replaced by the Dirac delta function $\delta[\varepsilon-\varepsilon_{\text{LB}}]$. Thus, we have:

$$\lambda_{Sa_{\text{avg}}(\mathbf{T}^*)=y} = \sum_{n=1}^{N_S} \sum_{k=1}^{N_M} \sum_{j=1}^{N_R} v_n \cdot \phi(\varepsilon_{\text{LB}}) \Delta\varepsilon \cdot P[R=r_j] \cdot P[M=m_k] \quad (11)$$

Now, by using the Bayesian theorem, the probability term, p_{jk}, can be expressed as follows:

$$p_{jk} = \frac{v_n \cdot \phi(\varepsilon_{\text{LB}}) \Delta\varepsilon \cdot P[R=r_j] \cdot P[M=m_k]}{\lambda_{Sa_{\text{avg}}(\mathbf{T}^*)=y,n}} \quad (12)$$

In the above equation, $\lambda_{Sa_{\text{avg}}(\mathbf{T}^*)=y,n}$ is the hazard associated with the nth seismic source, and again in this case $p_n = (\lambda_{Sa_{\text{avg}}(\mathbf{T}^*)=y,\,n} / \lambda_{Sa_{\text{avg}}(\mathbf{T}^*)=y})$. However, the important question is: "Which of the two expressions for p_{jk} should be employed in the estimation of the CS's distribution?". Baker and Cornell [7] proposed to carry out the deaggregation conditioned on meeting the target conditioning value, i.e., the definition of deaggregation by McGuire [12], rather than following alternate definition by Bazzurro and Cornell [18], where the deaggregation result is conditioned on the exceedance of the conditioned spectral acceleration. The McGuire [12] definition appears to be more reasonable due to the fact that the CS is conditioned on the equality of the spectral acceleration. However, the deaggregation results based on Bazzurro and Cornell [18] definition are more available

in practice. The discrepancy between the CS's distributions associated with the two definitions for deaggregation used in calculation of the probability term, p_{jk}, are further investigated in this study.

4. The approximate conditional spectra

The approximate CS has been introduced in this section since the exact solution requires incorporating a set of multiple causal M and R values from deaggregation analysis for a given $Sa_{\text{avg}}(\mathbf{T}^*)$ value, as described in the previous section. While the CS concept is considered for the practical use, the proper approximate methodologies need to be further explored in order to facilitate the hazard-consistent ground motion selection. Two different approximate approaches are presented in the current manuscript in order to calculate the CMS as followings:

(a) Compute the CMS associated with each seismic source using the mean M and R values of that source from the hazard deaggregation analysis, i.e., $\overline{M}_n,\overline{R}_n$. Then compute the CMS corresponding to all seismic sources using the contribution (weight) of each seismic source to exceedance or occurrence of conditioned $Sa_{\text{avg}}(\mathbf{T}^*)$ denoted as, p_n, which was defined in the previous section. The CMS calculated by this approach is denoted by $\ln Sa_{\text{CMS}}^{\text{app-}\overline{M}_n/\overline{R}_n}(T)$, and can be obtained as:

$$\ln Sa_{\text{CMS}}^{\text{app-}\overline{M}_n/\overline{R}_n}(T) = \mu_{\ln Sa(T)|\ln Sa_{\text{avg}}(\mathbf{T}^*)=x}^{\text{app-}\overline{M}_n/\overline{R}_n} = \sum_{n=1}^{N_S} p_n[\mu_{\ln Sa(T)}(\overline{M}_n,\overline{R}_n,\varphi_n)+\rho(T,\mathbf{T}^*)\cdot\overline{\varepsilon}_n\cdot\sigma_{\ln Sa(T)}] \tag{13}$$

The McGuire [12] definition of deaggregation was employed in Eq. (13) for estimation of p_n. Moreover, the value for $\overline{\varepsilon}_n$ can be calculated by two different approaches. First, using the lower bound epsilon defined in Eq. (4) by means of $\overline{M}_n$ and $\overline{R}_n$ values within the nth seismic source. Second, applying the mean value of epsilon associated with the nth seismic source, which can be calculated as follows:

$$\overline{\varepsilon}_n = \sum_{\varepsilon} \varepsilon\cdot P[\varepsilon|Sa_{\text{avg}}(\mathbf{T}^*)=y,\text{event}_n] \tag{14}$$

where,

$$P[\varepsilon|Sa_{\text{avg}}(\mathbf{T}^*)=y,\text{event}_n] = \frac{\sum_{k=1}^{N_M}\sum_{j=1}^{N_R} v_n\cdot\delta[\varepsilon-\varepsilon_{\text{LB}}]\phi(\varepsilon)\Delta\varepsilon\cdot P[R=r_j]\cdot P[M=m_k]}{\lambda_{Sa_{\text{avg}}(\mathbf{T}^*)=y,n}} \tag{15}$$

However, the application of the mean value for the epsilon will not necessarily lead to the predefined target $Sa_{\text{avg}}(\mathbf{T}^*)$ value. Therefore the conditional spectrum should then be scaled properly to meet this target conditional value. Consequently, the exact variance of CS expressed in Eq. (3) can further be approximated by considering the fact that the second term of this equation is eliminated according to this approximate approach. This approximate variance term, denoted by $\sigma^2_{\ln Sa_{\text{CMS}}^{\text{app-}\overline{M}_n/\overline{R}_n}(T)}$, can be expressed as:

$$\sigma^2_{\ln Sa_{\text{CMS}}^{\text{app-}\overline{M}_n/\overline{R}_n}(T)} = (\sigma_{\ln Sa(T)|\ln Sa_{\text{avg}}(\mathbf{T}^*)=x}^{\text{app-}\overline{M}_n/\overline{R}_n})^2 = (1-\rho^2(T,\mathbf{T}^*))\cdot\sum_{n=1}^{N_S} p_n\cdot\sigma^2_{\ln Sa(T)} \tag{16}$$

(b) Compute the CMS using the mean M and R values (i.e., $\overline{M}$, $\overline{R}$) from the total hazard deaggregation associated with all seismic sources (conventional approach).

$$\ln Sa_{\text{CMS}}^{\text{app-}\overline{M}/\overline{R}}(T) = \mu_{\ln Sa(T)|\ln Sa_{\text{avg}}(\mathbf{T}^*)=x}^{\text{app-}\overline{M}/\overline{R}} = \mu_{\ln Sa(T)}(\overline{M},\overline{R},\varphi)+\rho(T,\mathbf{T}^*)\cdot\overline{\varepsilon}\cdot\sigma_{\ln Sa(T)} \tag{17}$$

Again, the parameter $\overline{\varepsilon}$ can be estimated by the two pre-mentioned approaches, i.e., the lower bound epsilon estimated based on $\overline{M}$ and $\overline{R}$ values from the total hazard deaggregation, and the mean value of epsilon which equals:

$$\overline{\varepsilon} = \sum_{n=1}^{N_S} p_n\cdot\overline{\varepsilon}_n \tag{18}$$

Furthermore, the variance of the CS can be approximated as follows:

$$\sigma^2_{\ln Sa_{\text{CMS}}^{\text{app-}\overline{M}/\overline{R}}(T)} = (\sigma_{\ln Sa(T)|\ln Sa_{\text{avg}}(\mathbf{T}^*)=x}^{\text{app-}\overline{M}/\overline{R}})^2 = (1-\rho^2(T,\mathbf{T}^*))\cdot\sigma^2_{\ln Sa(T)} \tag{19}$$

Eqs. (17) and (19) were primarily proposed by Baker and Cornell [7,8] and Baker [9] for calculation of the CMS and its variance. It is worth mentioning that $\sigma_{\ln Sa(T)}$ is only a function of the respective period, T, in the current study, since the predictions were calculated at the level of the reference bedrock of the site; thus, both Eqs. (16) and (19) are identical. However, the equality between the variances of these two different approximations cannot be stated if the effect of the site-response terms is considered within the PSHA calculations.

5. Selection of the multi-seismic-sources region

The case-study offshore site is located in the South Pars Gas Field Development Phase-1 of the Persian Gulf region, 105 km from Assaluyeh (southern Iran) in 65 to 70 m water depth. The offshore facilities are located in the deforming zone separating Arabian Plate from the Eurasian Plate (Central Iran). The seismic hazard assessment for this site benefits from the past researches and specific studies carried out for examining seismo-tectonic characteristics as well as the historical earthquakes of the several sites in southern Iran ([25–29]; Noorzad A (2009), personal communication, University of Tehran, Iran).

According to these studies, the seismic sources considered in this research are comprised of four complex area sources, which are identified as a function of the tectonic deformation regime and the fault plane solution mechanism of earthquakes. These seismic sources were named ZMFF (Zagros Mountain Front Fault), ZFF-C (Central Zagros Fore-Deep Fault), PGMT (Persian Gulf Marginal Trough) which consists of background seismicity zone with scattered seismic activity, and ZCP-W (Zagros Coastal Plain-West). Different area sources were used in the current practice since the offshore site encompasses "background" seismicity zones in addition to the scattered and complex seismic activity associated with different seismic zones. The dominant deformation mechanisms are reverse with no-hanging wall effects.

Based on the seismicity of the case-study site, the mean annual rate of exceedance for the four suggested IMs, listed in Table 1, are shown in Fig. 1(a) along with 20 hazard curves associated with $Sa(T_i)$ where T_i denotes the 20-periods of the vector $\mathbf{T}^*$ logarithmically spaced in the interval of 0.5 to 4 s. The hazard curves were estimated at the bedrock level using the CB08 NGA model [24]. In addition, the Sa_{avg} level corresponding to the rare intense earthquake (R.I.E.), i.e., events with 2000-year return period [30], at the bedrock elevation equals to 0.08g for the first IM, i.e., Sa_{avg}(0.5 s,…,4 s), which is shown in Fig. 1(a), as well. The representative deaggregation that provides the distributions of

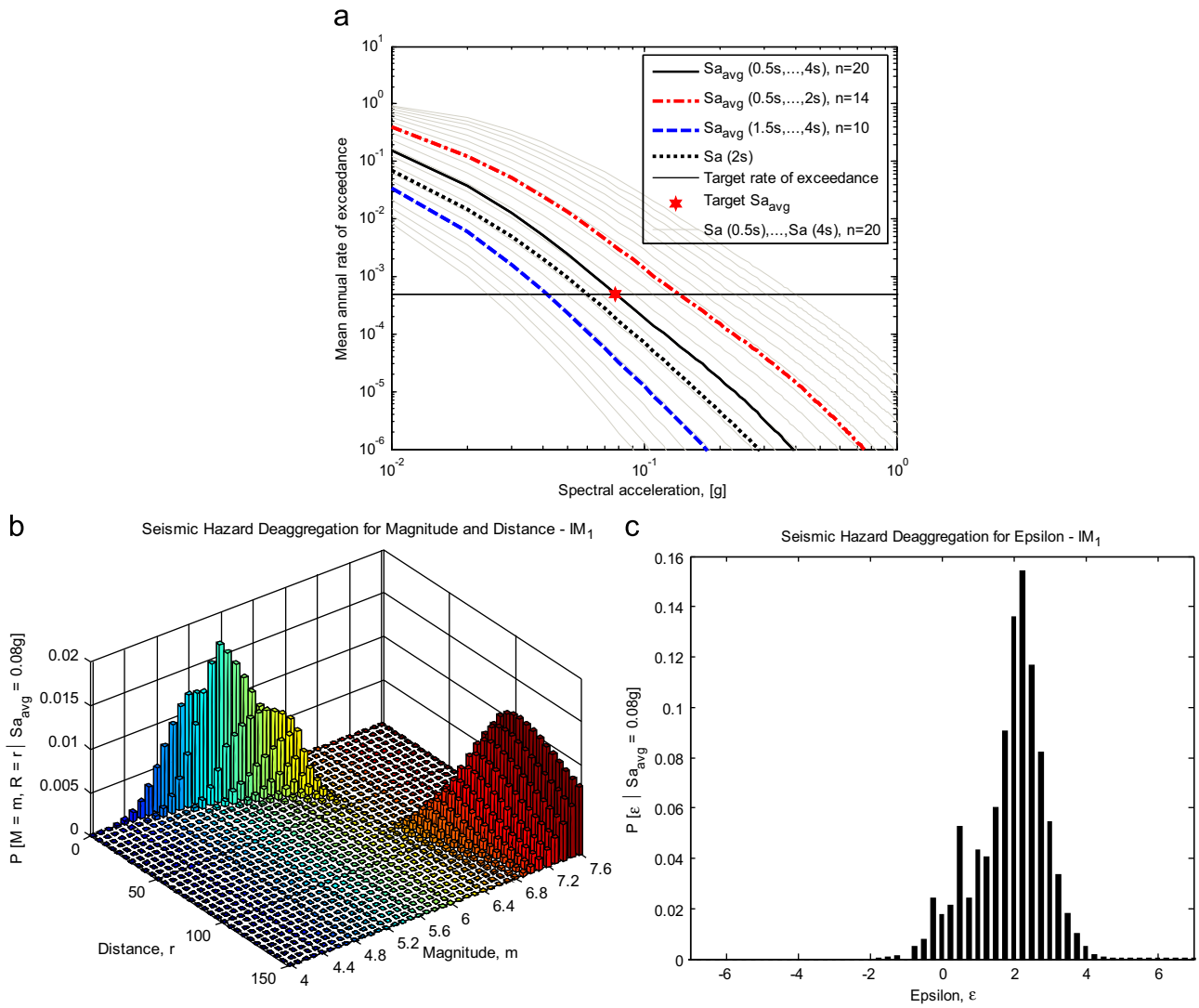

Fig. 1. (a) The PSHA curves for the four alternative IMs listed in Table 1 for the case-study site along with hazard curves associated with *Sa*'s at 20 logarithmically-spaced periods, all at the bedrock level using the CB08 NGA model; (b) and (c) PSHA deaggregation of magnitude, distance and epsilon given $Sa_{\text{avg}}(0.5\ s,\ldots,4\ s)=0.08g$.

magnitudes, distances, and epsilons given $Sa_{\text{avg}}(0.5s,\ \ldots,4s)=0.08g$ are shown in Fig. 1(b) and (c) based on McGuire [12] definition.

According to the deaggregation of magnitude and distance in Fig. 1(b), there are similar contributions from many comparable magnitude and distance bins which reveal the near-field sources with low magnitudes (i.e., ZCP-W and PGMT) as well as the far-field sources with high magnitudes (i.e., ZMFF and ZFF-C). Moreover, at this hazard levels, the deaggregation results in positive epsilon values for the near-field and low-magnitude as well as the far-field and high-magnitude events.

6. Calculation of the exact CS using different deaggregation approaches

The discrepancy between the mean and the standard deviation of the exact CS, given that the probability term p_{jk} associated with the hazard deaggregation in Eqs. (2) and (3) is conditioned on $Sa(T^*)=y$ and $Sa(T^*)>y$, are scrutinized in this section. It is worth noting that this section aims to explore these differences through the single-valued conditioning period, T^*. However, the same goal is provided further in this manuscript for the proposed IMs outlined in Table 1. The measure of dissimilarity is defined by means of the Averaged Sum of the Squared Errors (*ASSE*) by considering equally assigned weights, $w(T_j)$, to all periods of interest, as written in Eqs. (20) and (21):

$$ASSE_{\text{mean}}^{\text{deagg}}=\frac{\sum_{j=1}^{N_p} w(T_j)\cdot(\ln Sa_{\text{CMS}}^{\text{exact}|Sa(T^*)=y}(T_j)-\ln Sa_{\text{CMS}}^{\text{exact}|Sa(T^*)>y}(T_j))^2}{\sum_{j=1}^{N_p} w(T_j)}$$

$$=\frac{1}{N_p}\cdot\sum_{j=1}^{N_p}(\ln Sa_{\text{MS}}^{\text{exact}|Sa(T^*)=y}(T_j)-\ln Sa_{\text{CMS}}^{\text{exact}|Sa(T^*)>y}(T_j))^2 \tag{20}$$

$$ASSE_{\text{sigma}}^{\text{deagg}}=\frac{1}{N_p}\cdot\sum_{j=1}^{N_p}(\sigma_{\ln Sa_{\text{CMS}}^{\text{exact}|Sa(T^*)=y}(T_j)}-\sigma_{\ln Sa_{\text{CMS}}^{\text{exact}|Sa(T^*)>y}(T_j)})^2 \tag{21}$$

In the above equations, $ASSE_{\text{mean}}^{\text{deagg}}$ and $ASSE_{\text{sigma}}^{\text{deagg}}$ are, respectively, the *ASSE*s between the mean and the standard deviation values of $\ln Sa_{\text{CMS}}^{\text{exact}}$ conditioned on the single spectral value, $Sa(T^*)$, instead of $Sa_{\text{avg}}(\mathbf{T}^*)$ within Eqs. (2) and (3). Furthermore, $\ln Sa_{\text{CMS}}^{\text{exact}|Sa(T^*)=y}$ and $\sigma_{\ln Sa_{\text{CMS}}^{\text{exact}|Sa(T^*)=y}}$ are the mean and standard

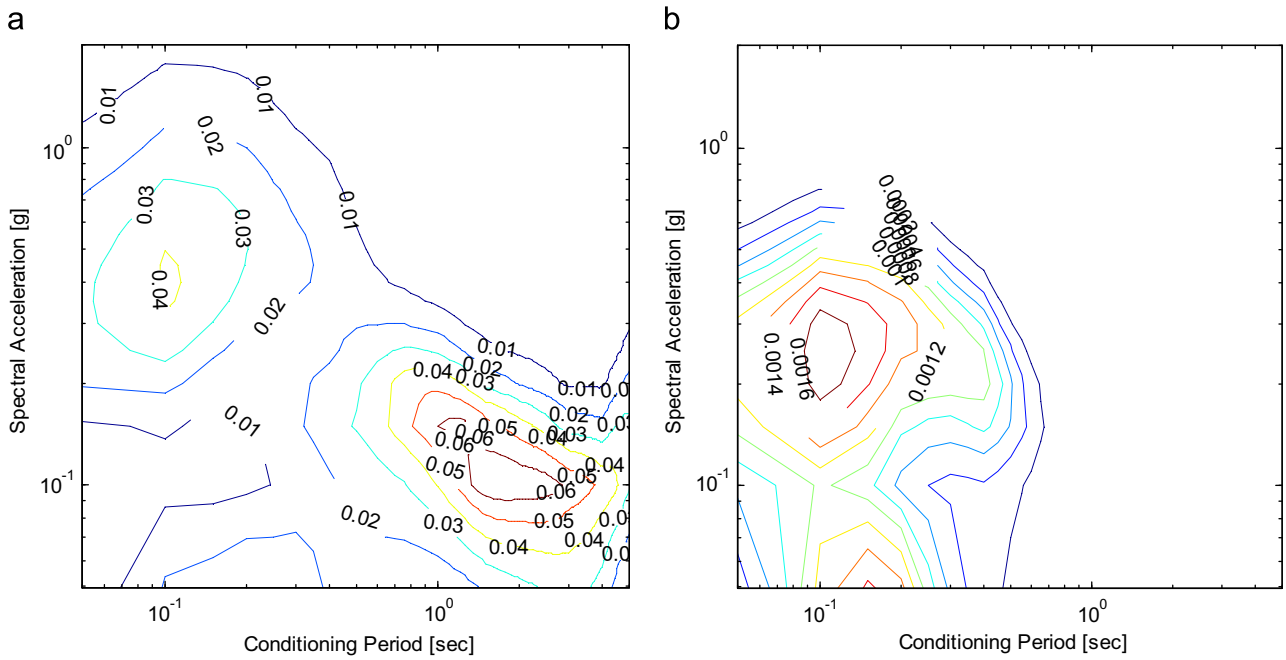

Fig. 2. The contours associated with (a) $ASSE_{\text{mean}}^{\text{deagg}}$, and (b) $ASSE_{\text{sigma}}^{\text{deagg}}$, for a range of conditioning period, T^*, and spectral accelerations, $Sa(T^*)$.

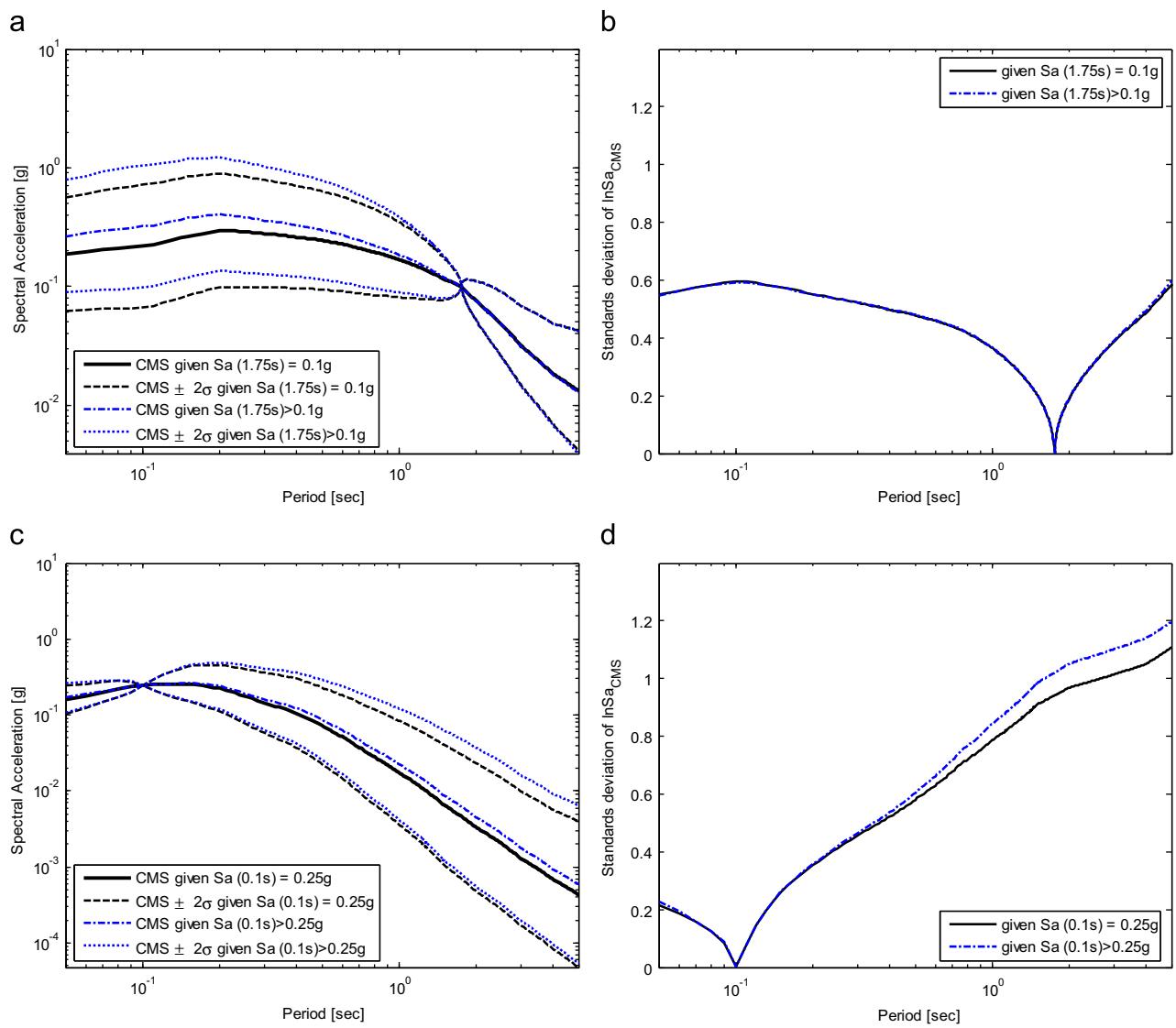

Fig. 3. The exact CMS and CMS $\pm 2\sigma$ as well as the standard deviation of CS given both definitions for PSHA deaggregation, where the CS is conditioned on (a) and (b) $Sa(1.75\text{ s})=0.1g$, (c) and (d) $Sa(0.1\text{ s})=0.25g$.

deviation of $\ln Sa_{\mathrm{CMS}}^{\mathrm{exact}}$ associated with the hazard deaggregation conditioned on $Sa(T^*)=y$, while $\ln Sa_{\mathrm{CMS}}^{\mathrm{exact}|Sa(T^*)>y}$ and $\sigma_{\ln Sa_{\mathrm{CMS}}^{\mathrm{exact}|Sa(T^*)>y}}$ are those related to the hazard deaggregation given $Sa(T^*)>y$. N_p denotes the number of periods considered which are logarithmically-spaced in the range of 0.01 to 5 s. Subsequently, Fig. 2 shows the contours of $ASSE_{\mathrm{mean}}^{\mathrm{deagg}}$ and $ASSE_{\mathrm{sigma}}^{\mathrm{deagg}}$ for a range of the single conditioning periods, T^*, and the spectral accelerations, $Sa(T^*)$ associated with the bedrock elevation.

According to Fig. 2, $ASSE_{\mathrm{mean}}^{\mathrm{deagg}}$ has the maximum value for the conditioning case of $Sa(1.75\ \mathrm{s})=0.1g$, while $ASSE_{\mathrm{sigma}}^{\mathrm{deagg}}$ is maximized in the case of $Sa(0.1\ \mathrm{s})=0.25g$. In order to have a deep insight into the discrepancy between the distributions of the exact CS given different definitions for deaggregation, the

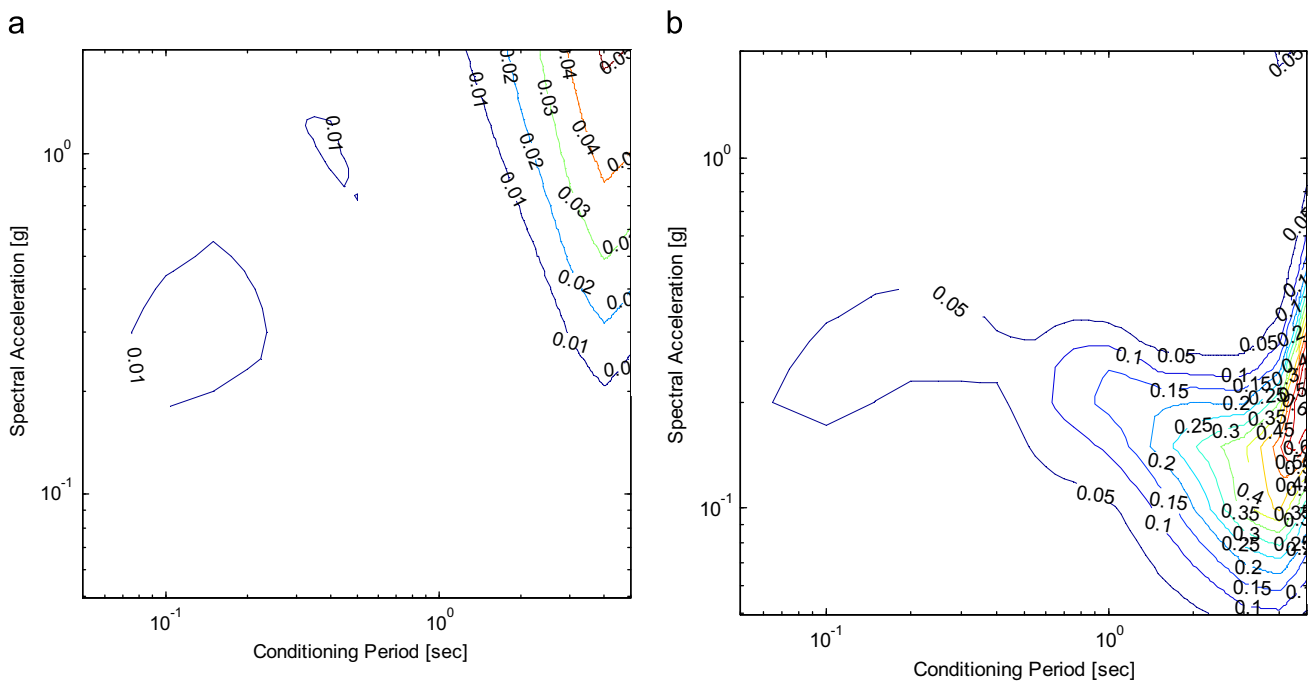

Fig. 4. The contours associated with (a) $ASSE_{\mathrm{mean}}^{\mathrm{app}\text{-}\overline{M}_n/\overline{R}_n}$, and (b) $ASSE_{\mathrm{mean}}^{\mathrm{app}\text{-}\overline{M}/\overline{R}}$, for a wide range of single conditioning periods, T^*, and spectral accelerations, $Sa(T^*)$, considering the lower-bound ε.

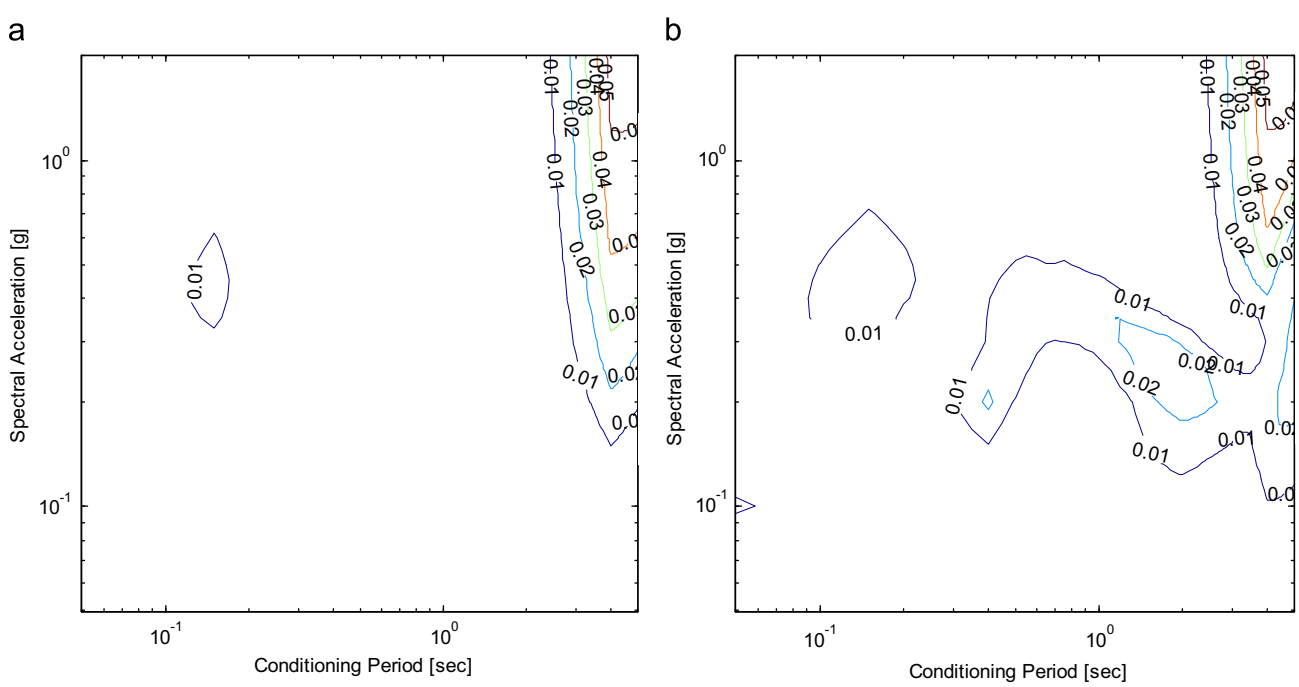

Fig. 5. The contours associated with (a) $ASSE_{\mathrm{mean}}^{\mathrm{app}\text{-}\overline{M}_n/\overline{R}_n}$, and (b) $ASSE_{\mathrm{mean}}^{\mathrm{app}\text{-}\overline{M}/\overline{R}}$, for a wide range of single conditioning periods, T^*, and spectral accelerations, $Sa(T^*)$, considering the mean-value ε.

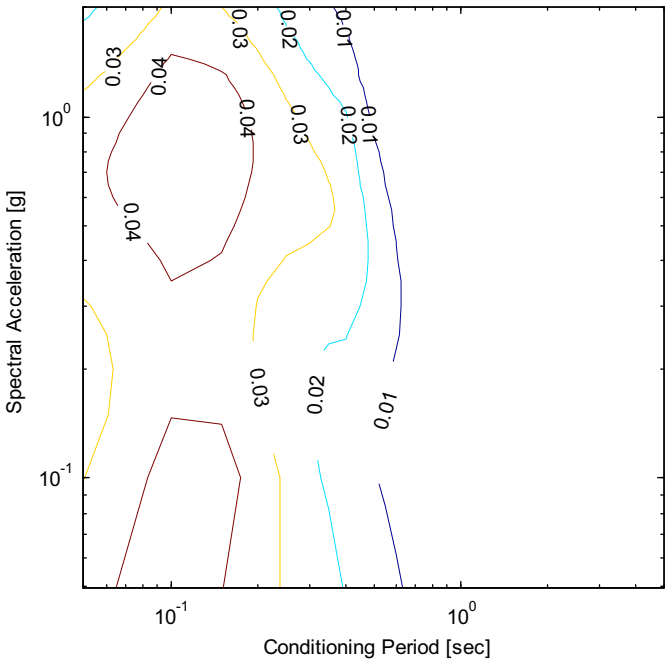

Fig. 6. The contours associated with $ASSE^{app}_{sigma}$, for a wide range of single conditioning periods, T^*, and spectral accelerations, $Sa(T^*)$.

distribution of the CS for both critical conditioning cases are shown in Fig. 3. It can be concluded that the distribution of the exact CS is affected by the employed deaggregation approach which is either based on $Sa(T^*)=y$ or $Sa(T^*)>y$. However, these results reveal that, at least for the given case-study offshore site, the selection of ground-motion records to match the CS's mean and variance is not substantially affected by each of the two definitions for deaggregation. However, for other sites with various seismic sources, more attention should be paid for the CS-based record selection in which the PSHA deaggregation is provided given that $Sa(T^*)>y$ in lieu of $Sa(T^*)=y$. In these certain conditions, the dissimilarity can become more apparent in the case of structural-response estimates.

It worth mentioning that the low *ASSE* values in the higher spectral acceleration region, as seen in Fig. 2, comes from this fact that a few significant M and R contribute to the hazard deaggregation and as a consequence the exact and approximate CMS are more similar to each other. On the other hand, several comparable M and R contribute to the hazard deaggregation when the spectral acceleration is low.

7. Comparing the exact and approximate distributions of CS

The *ASSE* is used again as a measure of dissimilarity between the exact and approximate mean and standard deviation of the CS

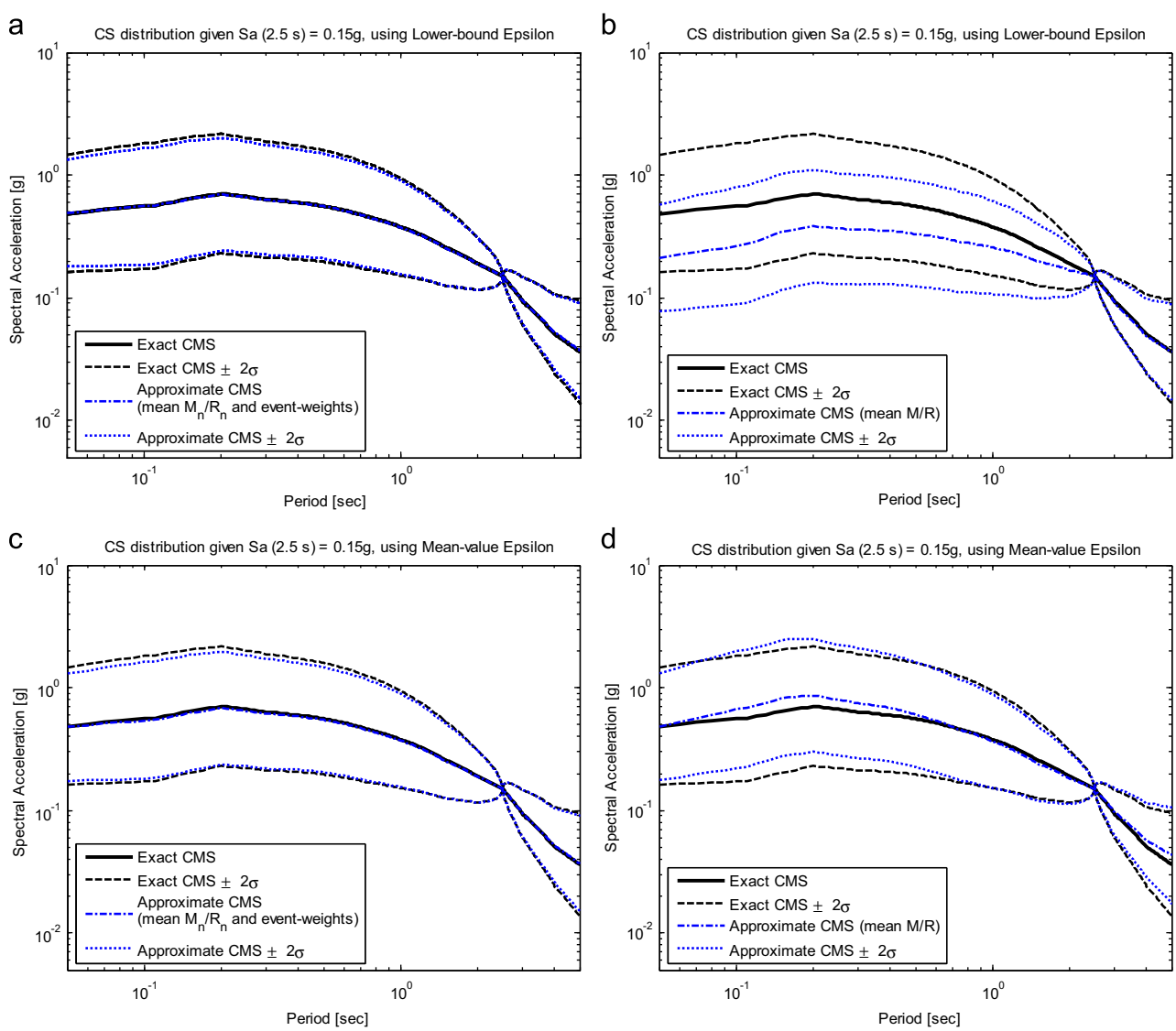

Fig. 7. The exact versus two approximate CMS and CMS $\pm 2\sigma$ associated with two selected critical conditioning cases within Fig. 4 including $Sa(2.5\text{ s})=0.15g$ by considering (a) and (b) lower-bound ε, (c) and (d) mean-value ε, and $Sa(0.15\text{ s})=0.30g$ by considering (e) and (f) lower-bound ε, (g) and (h) mean-value ε.

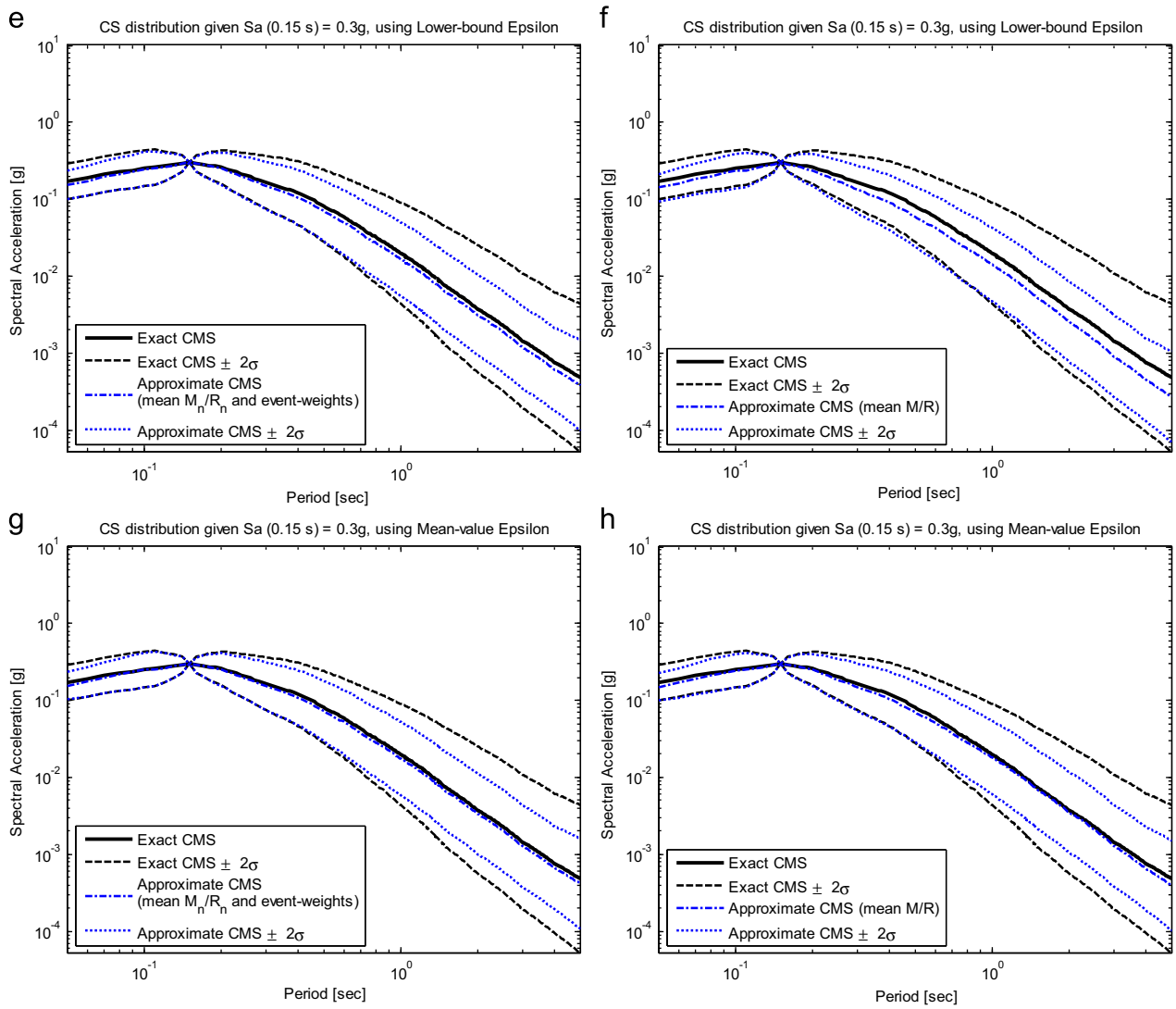

Fig. 7. (*continued*)

as written in Eqs. (22)–(24).

$$ASSE_{\text{mean}}^{\text{app-}\overline{M}_n/\overline{R}_n} = \frac{1}{N_p} \cdot \sum_{j=1}^{N_p} (\ln Sa_{\text{CMS}}^{\text{exact}}(T_j) - \ln Sa_{\text{CMS}}^{\text{app-}\overline{M}_n/\overline{R}_n}(T_j))^2 \tag{22}$$

$$ASSE_{\text{mean}}^{\text{app-}\overline{M}/\overline{R}} = \frac{1}{N_p} \cdot \sum_{j=1}^{N_p} (\ln Sa_{\text{CMS}}^{\text{exact}}(T_j) - \ln Sa_{\text{CMS}}^{\text{app-}\overline{M}/\overline{R}}(T_j))^2 \tag{23}$$

$$ASSE_{\text{sigma}}^{\text{app}} = \frac{1}{N_p} \cdot \sum_{j=1}^{N_p} (\sigma_{\ln Sa_{\text{CMS}}^{\text{exact}}(T_j)} - \sigma_{\ln Sa_{\text{CMS}}^{\text{app-}\overline{M}/\overline{R}}(T_j)})^2 \tag{24}$$

where $ASSE_{\text{mean}}^{\text{app-}\overline{M}_n/\overline{R}_n}$ and $ASSE_{\text{mean}}^{\text{app-}\overline{M}/\overline{R}}$ denote, respectively, the measure of dissimilarity between the exact CMS and the two CMS approximations within Eqs. (13) and (17). Furthermore, $ASSE_{\text{sigma}}^{\text{app}}$ corresponds to the average error in the standard deviation between the exact and each of the approximate levels. Since both approximate approaches for the standard deviation are identical in the case of the current study (see Eqs. (16) and (19)), only one error indicator was defined as shown in Eq. (24). Figs. 4–6 show the contours corresponding to these error estimators for a wide range of single conditioning periods, T^*, and the spectral acceleration values, $Sa(T^*)$ associated with the bedrock elevation. In the estimation of the different approximations for the CMS within Eqs. (22) and (23), the effect of both treatments of ε, i.e., lower-bound and mean-value ε's, were taken into account. Similar analyses were conducted later in the current study for different alternatives of $Sa_{avg}(\mathbf{T}^*)$ as the conditioning IMs, as well.

It can be observed, as seen in Figs. 4 and 5, that the error term $ASSE_{\text{mean}}^{\text{app-}\overline{M}/\overline{R}}$, while the lower-bound epsilon was utilized, is much higher than $ASSE_{\text{mean}}^{\text{app-}\overline{M}_n/\overline{R}_n}$ whereas these two terms reveal approximately the same order of errors in the case of the mean-value epsilon. Therefore, the most satisfactory conclusion is that both approximations, for the CMS estimation, are more similar when the mean-value epsilon is being used (i.e., Eqs. (13) and (17)). Moreover, as a general result, the approximate CMS based on $\overline{M}_n/\overline{R}_n$ and event-weights is more consistent with the exact CMS compared with the approximate CMS based on $\overline{M}/\overline{R}$. However, this difference is more significant, as seen in Figs. 4 and 5, in the case of the lower-bound epsilon. On the other side, when the major events of the site have different types of fault characteristics, which are represented by the parameter φ_n in this study, the choice of an appropriate value for the parameter φ, to be implemented in Eq. (17), is an important concern. As a result, when the hazard of the site originates from the diverse events

with different seismic characteristics, the CMS approximation by means of $\overline{M}_n/\overline{R}_n$ and event-weights seems to be more reasonable. This fact coincides with the findings extracted from Figs. 4 and 5. Furthermore, according to Fig. 6, a special attention should be paid in the calculation of the approximate CS, since the exact and approximate standard deviations have large discrepancy in the small range of conditioning periods, i.e., $T^* < 0.5$ s. Hence, for the small range of the conditioning periods, the approximate standard deviation (i.e., Eq. (19)) leads to lower estimates of the dispersion.

The distribution of the CS associated with the selected critical conditioning cases (see Figs. 4–6), which maximize the associated error terms are shown, respectively, in Figs. 7–9. It should further be noted that the critical areas within the contour lines, where the conditioning periods are beyond the limits for the applications in the engineering practice associated with the case study offshore site, were not considered herein.

The different critical cases of the conditioning spectral acceleration, $Sa(T^*)$, in which the approximate distribution of CS lead to striking dissimilarities with the associated exact solution, has been investigated through Figs. 7–9. It is again proved, as seen in Figs. 7 and 9, that the proposed approximations of the CS's distribution can significantly deviate from the exact estimates for the specific conditioning values (see e.g., Fig. 7(b), (e)–(h), Fig. 8(d), and Fig. 9). As a result, the approximate CS, especially those which were calculated based on $\overline{M}_n/\overline{R}_n$ and the lower-bound epsilon as well as those in the small range of conditioning periods, i.e., $T^* < 0.5$ s, can significantly affect the selected ground-motion records for the dynamic structural analysis within various levels of (conditioning) $Sa(T^*)$.

8. Comparing the exact and approximate CS for different conditioning IMs

The discrepancy between the exact means and the standard deviations of the CS conditioned on each of the alternative IMs in Table 1, given that the deaggregation is conditioned on exceeding or meeting the target average spectral acceleration value, $Sa_{\mathrm{avg}}(\mathbf{T}^*)$, were estimated by means of Eqs. (20) and (21). Therefore, the error estimators, $ASSE_{\mathrm{mean}}^{\mathrm{deagg}}$ and $ASSE_{\mathrm{sigma}}^{\mathrm{deagg}}$, were calculated for a range of $Sa_{\mathrm{avg}}(\mathbf{T}^*)$ values as shown in Fig. 10, while the vectors for $\mathbf{T}^*$ associated with different IMs were already reported in Table 1.

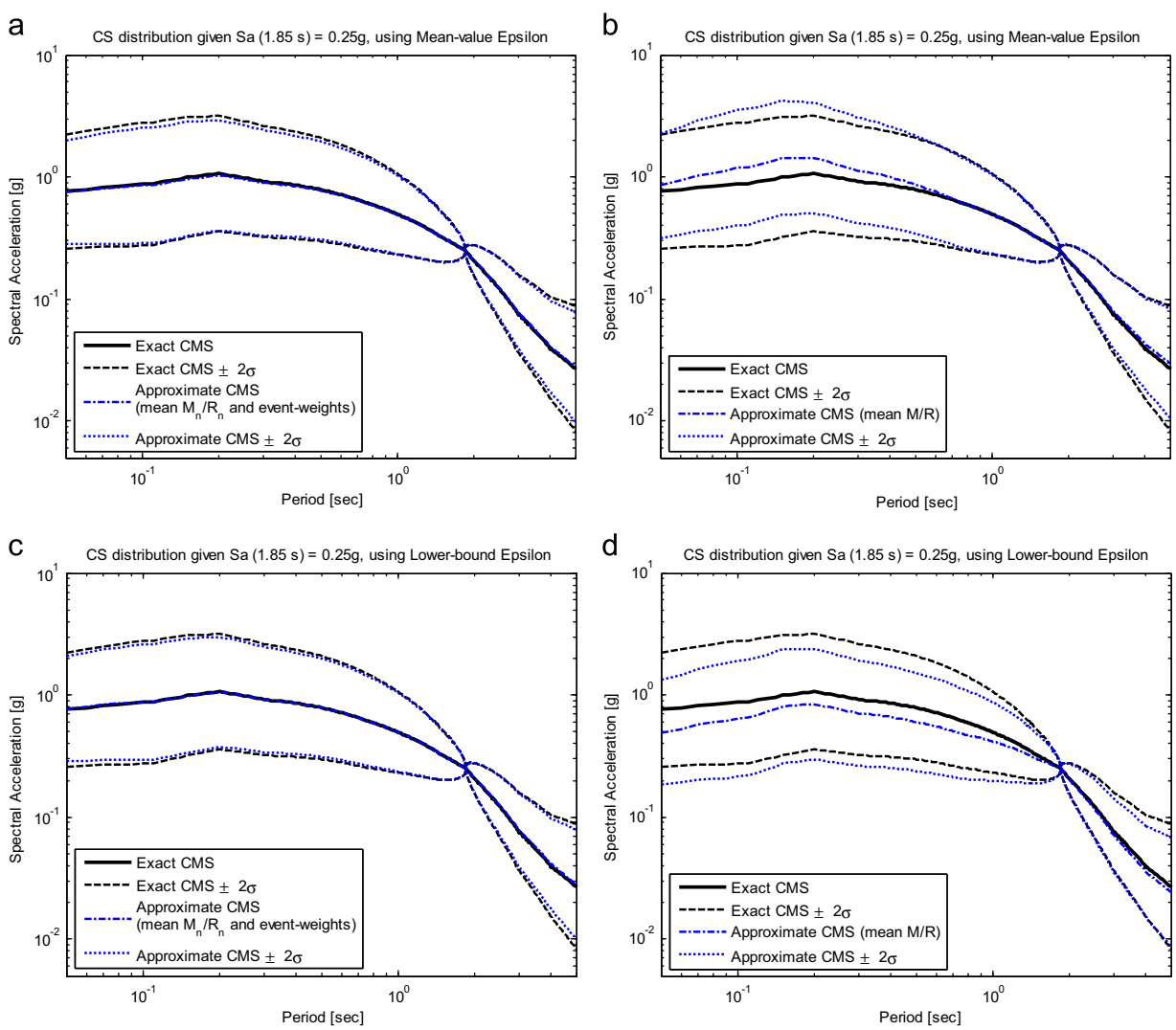

Fig. 8. The exact versus two approximate CMS and CMS $\pm 2\sigma$ associated with a selected critical conditioning case within Fig. 5 including $Sa(1.85\text{ s})=0.25g$ considering (a) and (b) mean-value ε, (c) and (d) lower bound ε.

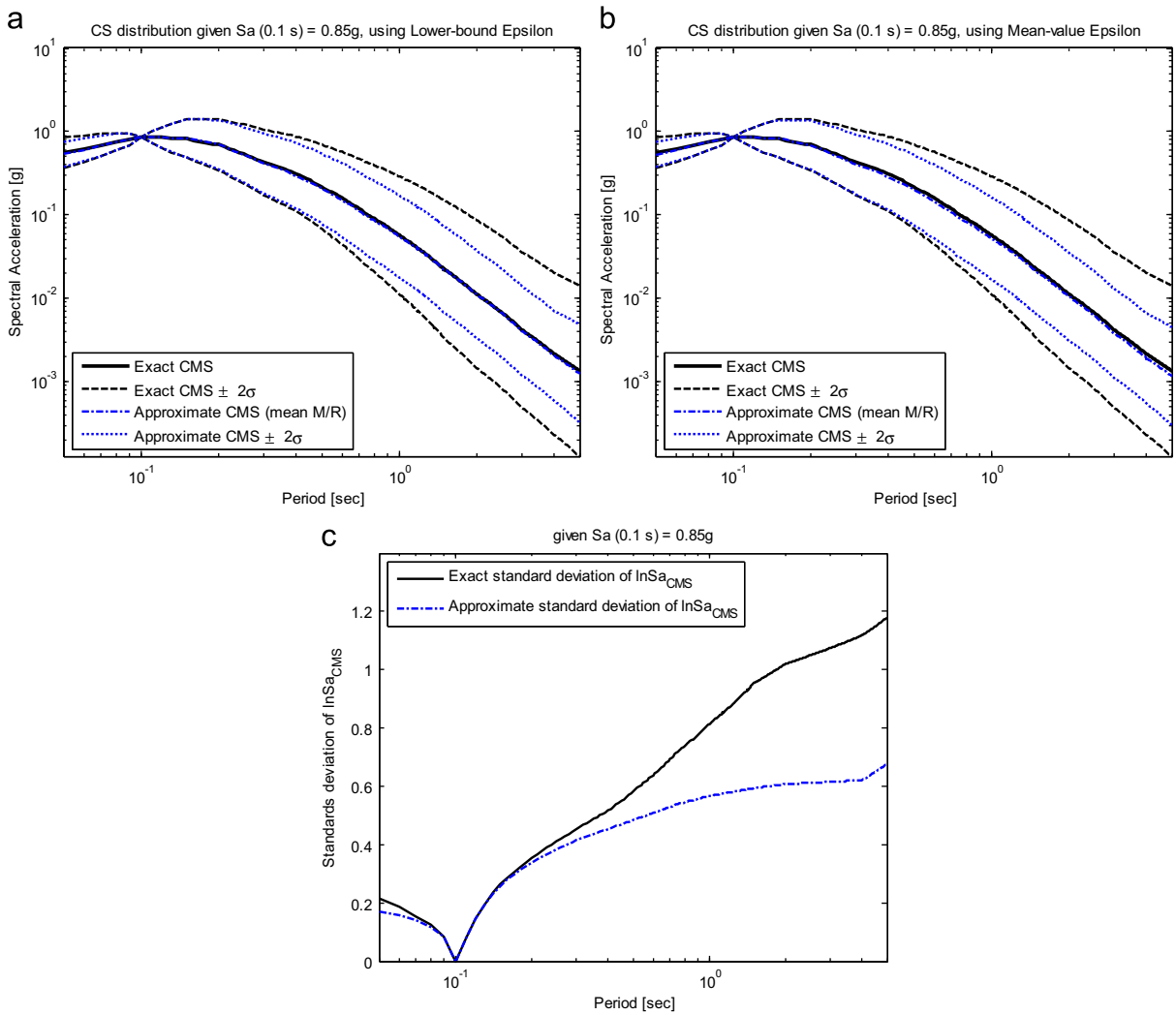

Fig. 9. The exact versus approximate CMS and CMS $\pm 2\sigma$ by considering (a) lower-bound ε, (b) mean-value ε, and (c) standard deviation of the exact versus approximate CS, all associated with a selected critical conditioning case of $Sa(0.1\text{ s})=0.85g$ within Fig. 6.

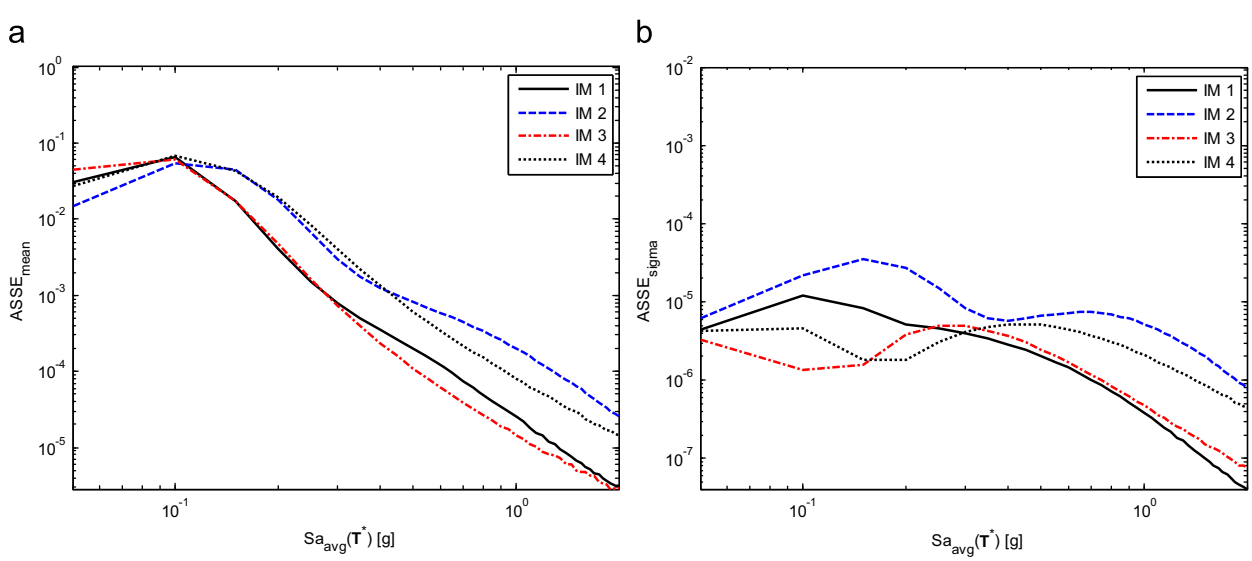

Fig. 10. (a) $ASSE_{\text{mean}}^{\text{deagg}}$, and (b) $ASSE_{\text{sigma}}^{\text{deagg}}$, for a range of $Sa_{\text{avg}}(\mathbf{T}^*)$ values associated with different IMs.

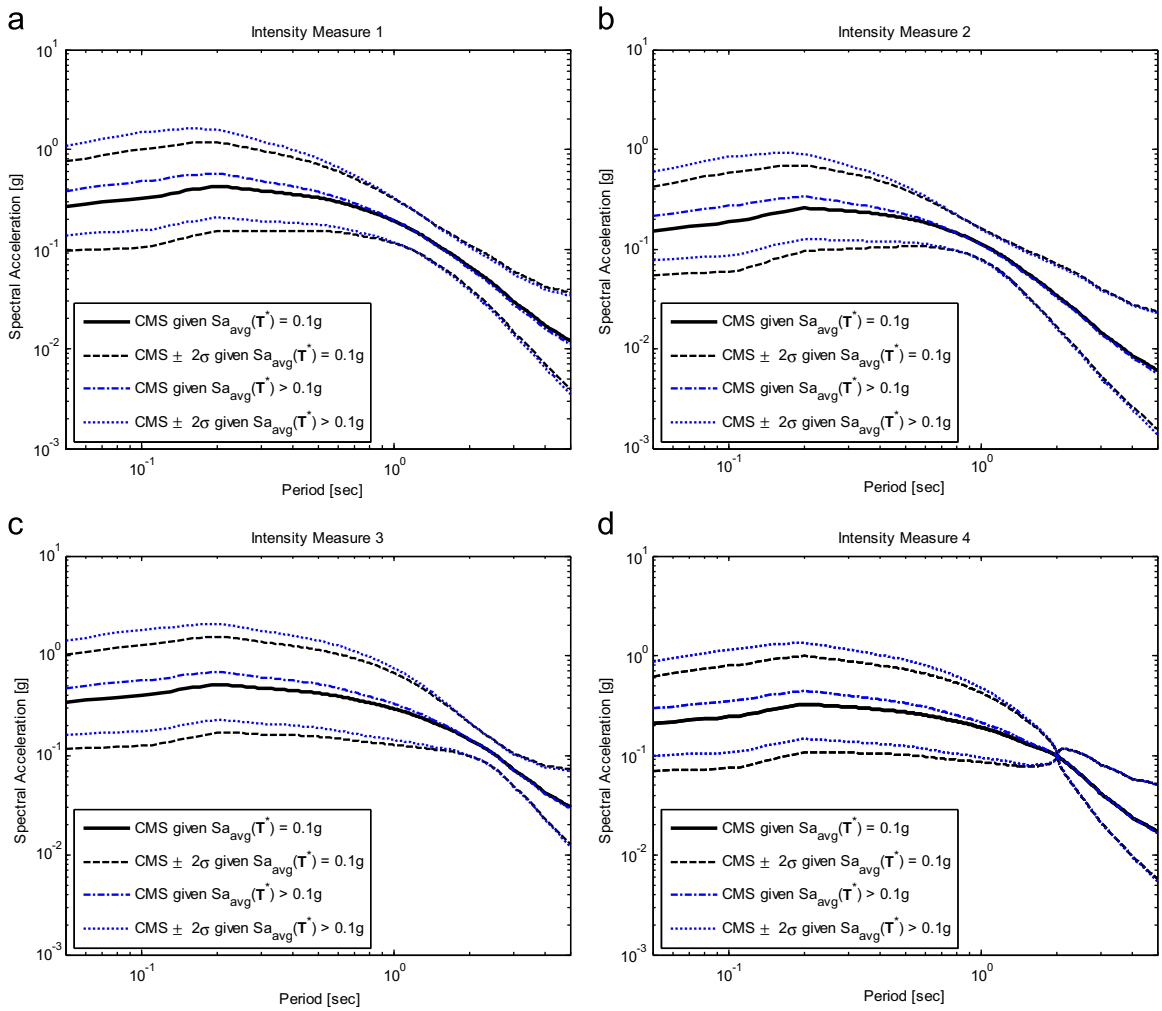

Fig. 11. The exact CMS and CMS $\pm 2\sigma$ for the conditioning case $Sa_{\mathrm{avg}}(\mathbf{T}^*)=0.1g$ given both deaggregation methodologies considering four selected IMs in Table 1 – (a) IM 1, (b) IM 2, (c) IM 3, and (d) IM 4.

The trend shown in Fig. 10(a) is consistent with that shown in Fig. 2(a), which shows the contour of $ASSE_{\mathrm{mean}}^{\mathrm{deagg}}$ for a range of the single conditioning periods, T^*, and the spectral accelerations, $Sa(T^*)$. According to Fig. 10(a), it can be depicted that $ASSE_{\mathrm{mean}}^{\mathrm{deagg}}$ is maximized for the target conditioning Sa value around $0.1g$, and further becomes smaller at higher spectral acceleration rates. Since $ASSE_{\mathrm{sigma}}^{\mathrm{deagg}}$ in Fig. 2(b) is sensitive to $T^* < 0.5$ s, the standard deviations of the exact CS, associated with both deaggregation approaches in Fig. 10(b), reveal minor differences in a wide range of conditioning IMs for the reason that all Sa_{avg} values are averaged on periods larger than 0.5 s. Subsequently, the distribution of the CS, for the critical conditioning case $Sa_{\mathrm{avg}}(\mathbf{T}^*)=0.1\mathrm{g}$, which maximizes the error terms $ASSE_{\mathrm{mean}}^{\mathrm{deagg}}$ for all IMs, are shown in Fig. 11.

Again, Fig. 11 implies that the exact CS, conditioned on each of the alternative IMs in Table 1, is affected by the two different deaggregation definitions. As a general result for other sites with various seismic sources, the CS based on the PSHA deaggregation conditioned on the exceedance of the target spectral value should be utilized with great attention.

To further investigate the effect of different approximate approaches, introduced in Section 4, for estimating the CS conditioned on each of the IMs in Table 1, the error estimators $ASSE_{\mathrm{mean}}^{\mathrm{app}\text{-}\overline{M}_n/\overline{R}_n}$, $ASSE_{\mathrm{mean}}^{\mathrm{app}\text{-}\overline{M}/\overline{R}}$, and $ASSE_{\mathrm{sigma}}^{\mathrm{app}}$ within Eqs. (22)–(24) were calculated for a range of $Sa_{\mathrm{avg}}(\mathbf{T}^*)$ values and different ε's definitions as shown in Fig. 12.

According to Fig. 12(a)–(d), the error term $ASSE_{\mathrm{mean}}^{\mathrm{app}\text{-}\overline{M}_n/\overline{R}_n}$, when the lower-bound epsilon is utilized, appears to be more substantial in the considered range of the alternative IMs. In addition, the error term $ASSE_{\mathrm{mean}}^{\mathrm{app}\text{-}\overline{M}_n/\overline{R}_n}$ has a smaller amount compared to $ASSE_{\mathrm{mean}}^{\mathrm{app}\text{-}\overline{M}_n/\overline{R}_n}$ regardless of the type of ε's definitions. It is worth noting that the trend shown in these figures are entirely consistent with those shown in Figs. 4 and 5; $ASSE_{\mathrm{mean}}^{\mathrm{app}\text{-}\overline{M}_n/\overline{R}_n}$ increases as the conditioning IM intensifies according to Figs. 4(a) and 5(a), no matter which definition of ε is used. Subsequently, $ASSE_{\mathrm{mean}}^{\mathrm{app}\text{-}\overline{M}_n/\overline{R}_n}$ using lower-bound epsilon is maximized for the target conditioning Sa values between $0.1g$ and $0.2g$ (Fig. 4(b)), while it is sensitive to $Sa > 0.1g$ regarding mean-value epsilon (see Fig. 5(b)). However, all of these results are more evident for $T^* > 1$ s; hence, the third IM in Table 1, i.e., $Sa_{\mathrm{avg}}(1.5\text{ s},\ldots,4\text{ s})$ has the highest value in the critical IM range, while the second IM, i.e., $Sa_{\mathrm{avg}}(0.5\text{ s},\ldots,2\text{ s})$ has the lowest value. Furthermore, based on Fig. 12(d), $ASSE_{\mathrm{sigma}}^{\mathrm{app}}$ follows the same trend for different IMs and both exact and approximate standard deviations of the CS have a small discrepancy for the four considered IMs. However, the maximum $ASSE_{\mathrm{sigma}}^{\mathrm{app}}$ arises generally from the second IM, i.e., $Sa_{\mathrm{avg}}(0.5\text{ s},\ldots,2\text{ s})$, which includes the range of low-conditioning periods. This result is in line with the findings in Fig. 6 where the

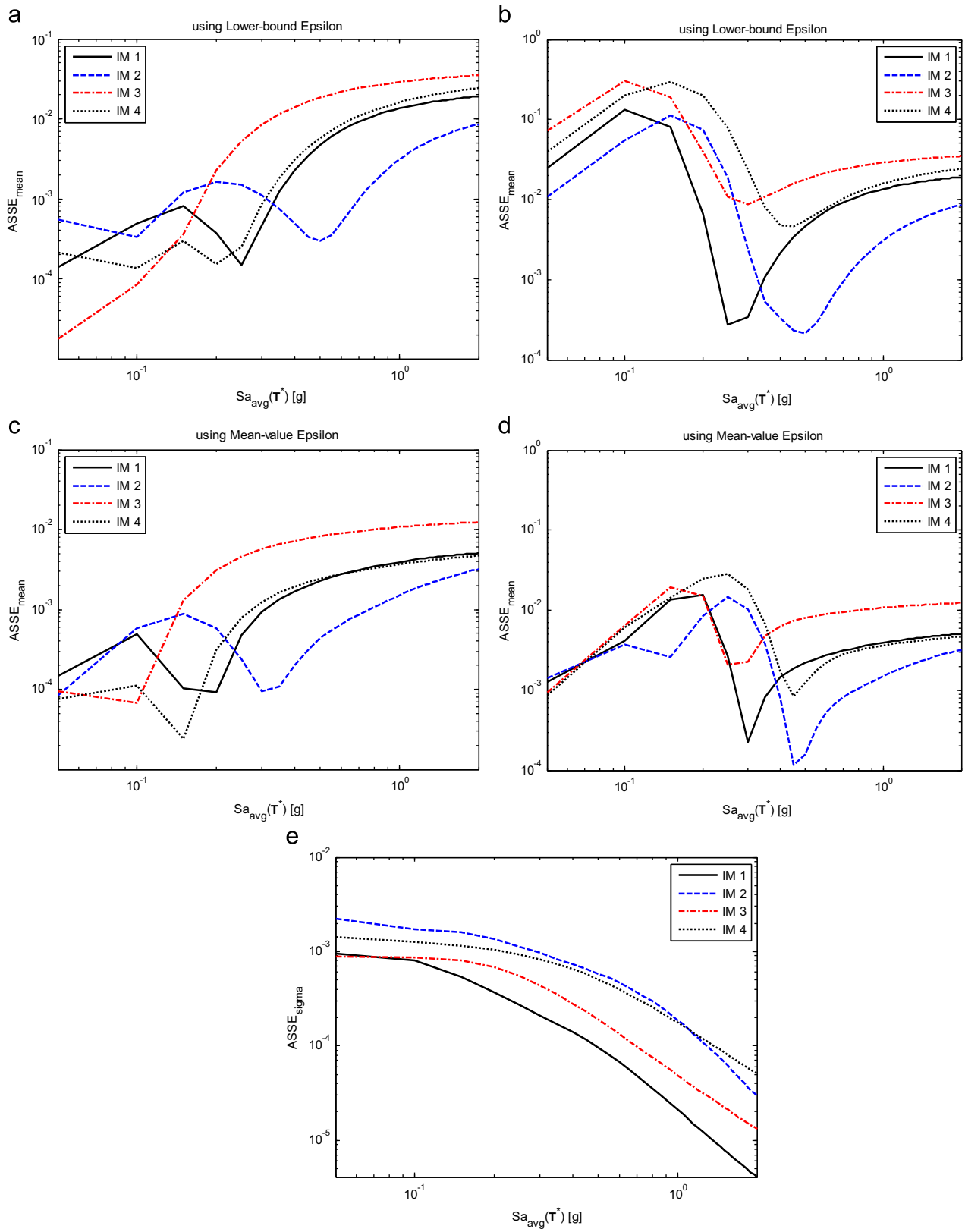

Fig. 12. (a) $ASSE_{\text{mean}}^{\text{app-}\overline{M}_n/\overline{R}_n}$, and (b) $ASSE_{\text{mean}}^{\text{app-}\overline{M}/\overline{R}}$, considering the lower-bound ε, (c) $ASSE_{\text{mean}}^{\text{app-}\overline{M}_n/\overline{R}_n}$, and (d) $ASSE_{\text{mean}}^{\text{app-}\overline{M}/\overline{R}}$, considering the mean-value ε, (e) $ASSE_{\text{sigma}}^{\text{app}}$, all for a range of $Sa_{\text{avg}}(\mathbf{T}^*)$ values.

approximate standard deviation had considerable dissimilarity compared with the exact one in the small range of single conditioning periods (i.e., below 0.5 s). Subsequently, the distribution of the CS associated with different critical conditioning cases of $Sa_{\text{avg}}(\mathbf{T}^*)$, which maximize the error term $ASSE^{\text{app-}\overline{M}/\overline{R}}$, are shown in Figs. 13–15. In Figs. 13 and 14, 'Approximate CMS

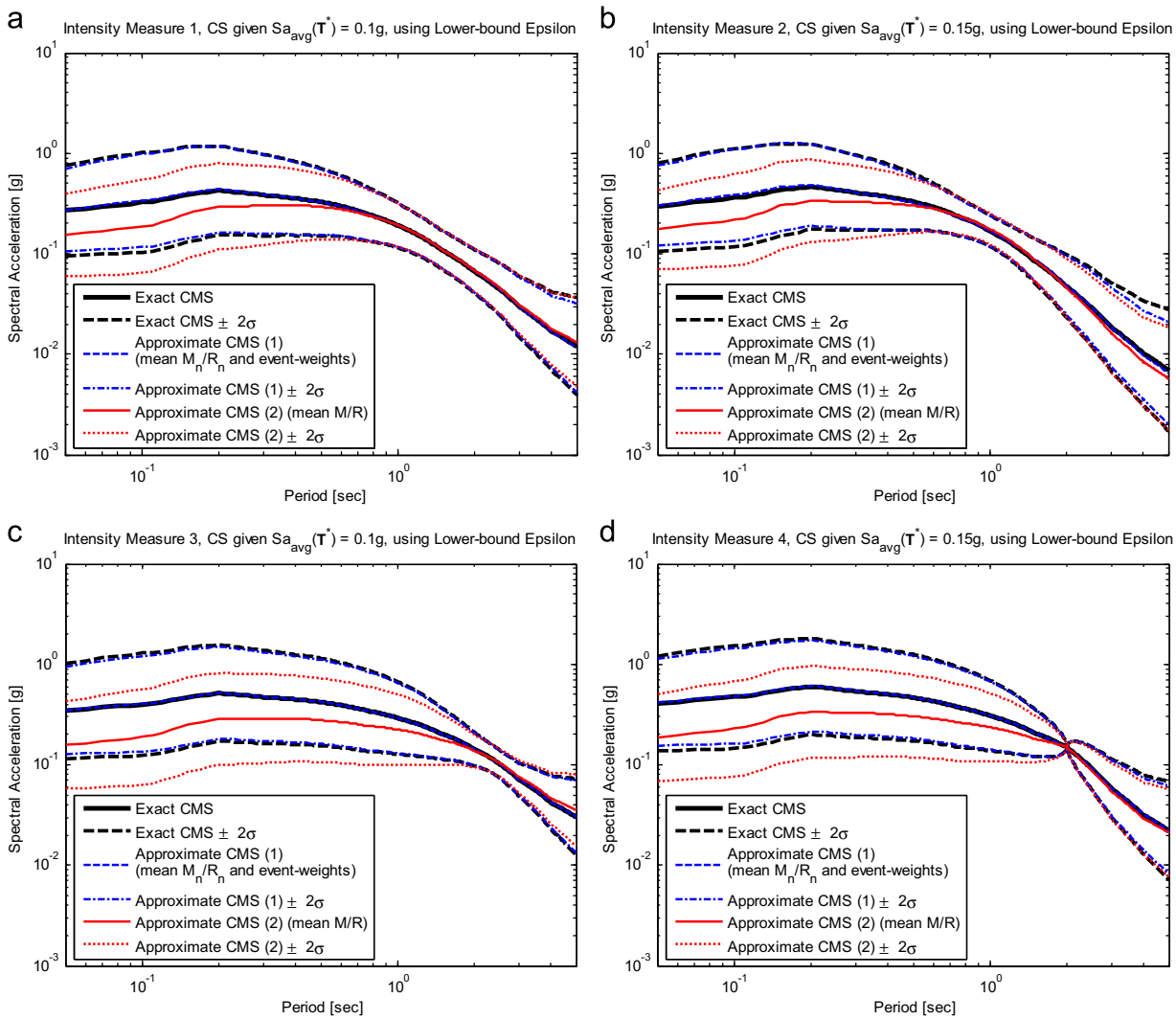

Fig. 13. The exact versus two approximate CMS and CMS $\pm 2\sigma$ for critical conditioning cases of $Sa_{\text{avg}}(\mathbf{T}^*)$ considering four selected IMs in Table 1 – (a) IM 1, (b) IM 2, (c) IM 3, and (d) IM 4, by utilizing the the lower-bound ε.

(1)' denotes approach (a) in Section 4, where the CMS associated with each seismic source using $\overline{M}_n/\overline{R}_n$ are combined by the weight factor p_n. Subsequently, 'Approximate CMS (2)' stands for approach (b), in which the CMS is computed using $\overline{M}/\overline{R}$ associated with all seismic sources, also known as the conventional method.

Accordingly, the same results, as those previously found in Section 7, can be obtained which are summarized as:

- Utilizing the mean-value epsilon in both approximations of the CMS results in the estimates that are much more analogous to the exact CMS. This is due to the fact that using the mean-value epsilon needs scaling since the CMS do not actually meet the target conditioning $Sa_{\text{avg}}(\mathbf{T}^*)$ level, as discussed previously. However, this scaling can adjust the CMS in its entire period-range to become more similar to the exact CMS. While using the lower-bound epsilon, this adjustment will be localized.
- The approximate CMS calculated based on $\overline{M}_n/\overline{R}_n$ with event-weights appears to be more similar to the exact CMS compared to that calculated according to $\overline{M}/\overline{R}$.
- The exact and approximate standard deviations of CS have small discrepancy for the four IMs considered herein.
- The approximate CMS with $\overline{M}/\overline{R}$ utilizing the lower-bound epsilon, can significantly deviate from the exact estimates.

It is worth emphasizing that all the obtained results are conducted with respect to the considered example limitations. More investigations are needed in order to globalize the results.

9. Conclusion

The exact and two different approximate conditional spectra are compared in this manuscript for a given multi-seismic-sources offshore site in the South Pars Gas Field located in the Persian Gulf region in southern Iran. As the deaggregation results confirm, the considered site has been influenced by the multiple comparable seismic sources which means that a simple seismic source (M and R) can produce bias in estimating the distribution of the conditional spectrum. The first approximate approach computes the distribution of the conditional spectrum for each seismic source individually by utilizing the mean M and R values associated with each source from the probabilistic seismic hazard deaggregation (i.e., $\overline{M}_n,\overline{R}_n$). Then, the mean and the standard

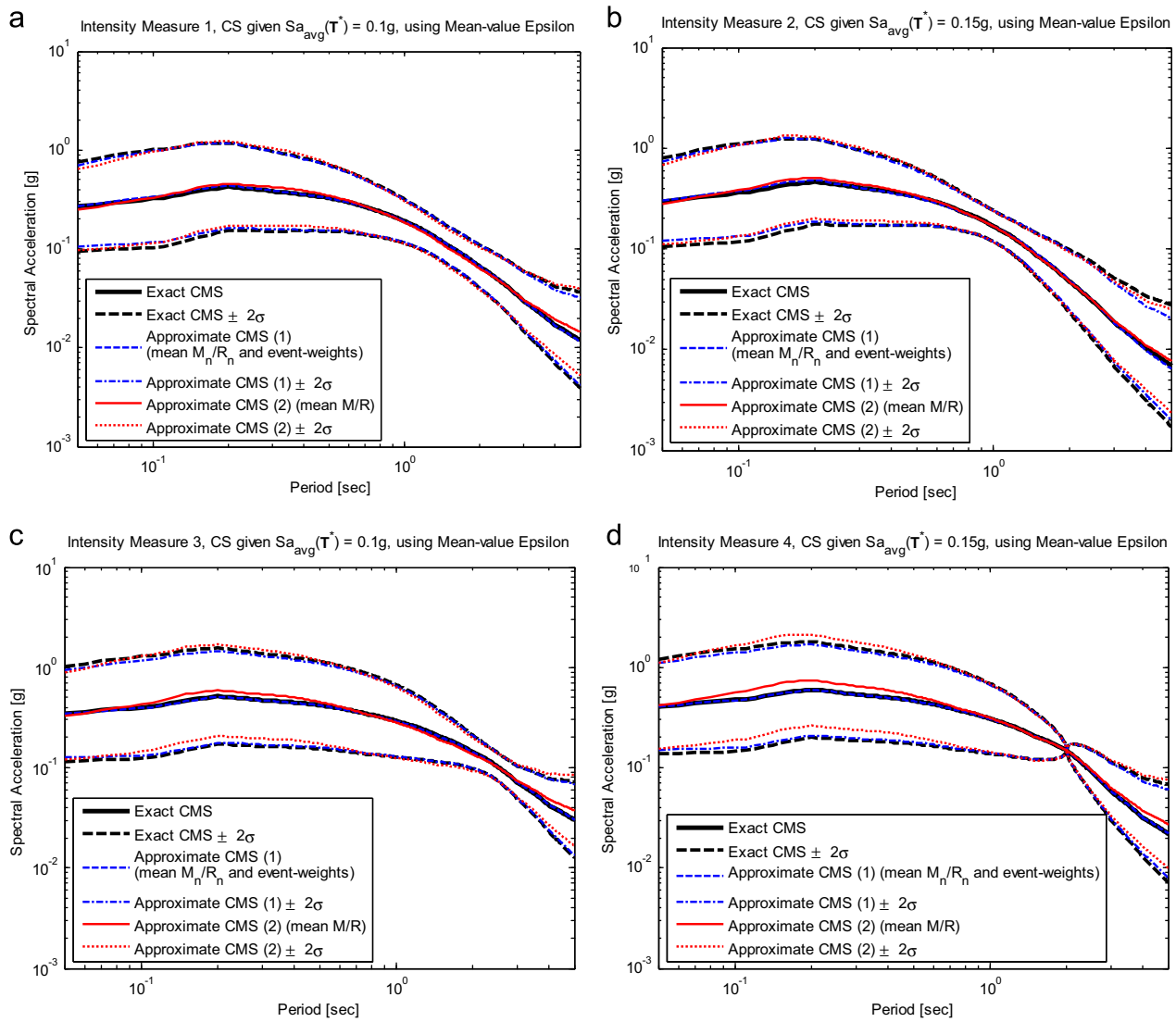

Fig. 14. The exact versus two approximate CMS and CMS $\pm 2\sigma$ for critical conditioning cases of $Sa_{avg}(\mathbf{T}^*)$ considering four selected IMs in Table 1 – (a) IM 1, (b) IM 2, (c) IM 3, and (d) IM 4, by utilizing the mean-value ε.

deviation of the target conditional spectrum corresponding to all seismic sources are estimated by summing these individual values using the weight of each seismic source. However, the second (conventional) approach calculates the distribution of the conditional spectrum using the mean M and R values from the total hazard deaggregation (i.e., $\overline{M},\overline{R}$) associated with all seismic sources. In addition, two distinct approaches for calculation of $\bar{\varepsilon}$ within each approximate approach were considered, i.e., the lower-bound epsilon and the mean-value epsilon.

Based on the results of this study, it can be revealed that the first proposed approximate approach can lead to the spectral shape of the conditional mean spectrum that has a small deviation from the exact solution compared to the second approach (i.e., the conventional method). In addition, the conditional mean spectra calculated based on the mean-value epsilon were more reasonable than those using the lower-bound epsilon. Nevertheless, the most satisfactory conclusion that can generally be drawn in this study is that the conditional mean spectrum calculated by the second proposed approximate approach, while the lower-bound epsilon is utilized, can significantly deviate from the exact estimates. Furthermore, for the small range of the conditioning periods, i.e., $T^* < 0.5$ s, the approximate standard deviation of the conditional spectra leads to lower estimates of the dispersion.

The exact distribution of the conditional spectrum by utilizing two different definitions for deaggregation analysis, which are based on exceeding or meeting the target spectral acceleration, i.e., $Sa(T^*) > y$ and $Sa(T^*) = y$, were compared in this study. As a result, the distributions of the conditional spectra, at least for the given case-study offshore site, were not substantially affected by each of the two definitions for deaggregation. However, for other sites with various seismic sources, meticulous attention should be paid while the deaggregation results are provided given that $Sa(T^*) > y$ in lieu of $Sa(T^*) = y$.

The effects of different approximations as well as definitions of the deaggregation on the distribution of the conditional spectrum, by means of four different intensity measures, were examined in this study. These intensity measures were comprised of the spectral acceleration at a specified period as well as alternative intensity measures which were defined based on the spectral acceleration averaged over different ranges of periods. The results show that the proposed approximate approach can be a good

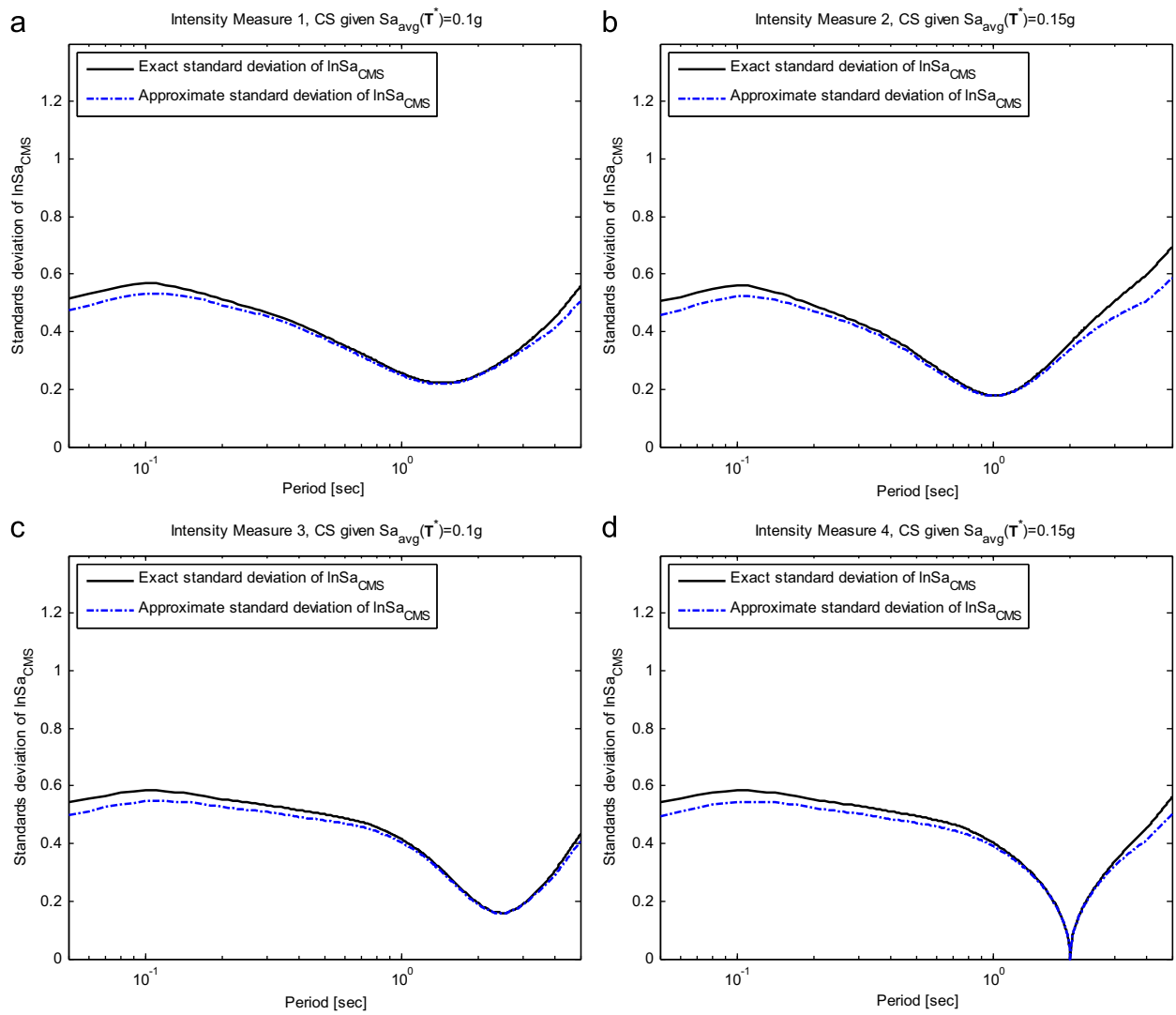

Fig. 15. Standard deviation of the exact versus approximate CS for critical conditioning cases of $Sa_{avg}(\mathbf{T}^*)$ for the four selected IMs in Table 1 – (a) IM 1, (b) IM 2, (c) IM 3, and (d) IM 4.

representative of the exact solution in all four different intensity measures.

Acknowledgments

This research was primarily supported by the Research and Development Department of Pars Oil and Gas Company (POGC) subsidiary of National Iranian Oil Company (NIOC) under contract number 123/PT. This support is gratefully acknowledged. The authors are also very grateful to both anonymous reviewers for their valuable comments.

References

[1] International Code Council (ICC). International Building Code. Building Officials and Code Administrators International, Inc., Country Club Hills, IL; International Conference of Building Officials, Whittier, CA; and Southern Building Code Congress International, Inc., Birmingham, AL, 2000.
[2] CEN. Eurocode 8 design of structures for earthquake resistance. Part 1: General rules, seismic actions and rules for buildings. Final Draft prEN 1998, European Committee for Standardization, Brussels, 2003.
[3] ASCE. Minimum design loads for buildings and other structures. ASCE Standard No. 007-05, American Society of Civil Engineers, 2006.
[4] FEMA. NEHRP Recommended Provisions for Seismic Regulations for New Buildings and Other Structures.2000 edn., Part 1. Washington, DC: FEMA 368, Building Seismic Safety Council for the Federal Emergency Management Agency; 2001.
[5] Naeim F, Lew M. On the use of design spectrum compatible time histories. Earthquake Spectra 1995;11(1):111–27.
[6] Bommer JJ, Scott SG, Sarma SK. Hazard-consistent earthquake scenarios. Soil Dynamics and Earthquake Engineering 2000;19(4):219–31.
[7] Baker JW, Cornell CA. Vector-valued ground motion intensity measures for probabilistic seismic demand analysis. John A. Blume Earthquake Engineering Center, Report No. 150, Stanford University, Stanford, CA, 2005:321 pp.
[8] Baker JW, Cornell CA. Spectral shape, epsilon and record selection. Earthquake Engineering and Structural Dynamics 2006;35(9):1077–95.
[9] Baker JW. The conditional mean spectrum: a tool for ground motion selection. Journal of Structural Engineering, ASCE 2011;137(3):322–31.
[10] Baker JW, Cornell CA. A vector-valued ground motion intensity measure consisting of spectral acceleration and epsilon. Earthquake Engineering and Structural Dynamics 2005;34(10):1193–217.
[11] Mousavi M, Ghafory-Ashtiany M, Azarbakht AR. A new indicator of elastic spectral shape for more reliable selection of ground motion records. Earthquake Engineering and Structural Dynamics 2011;40:1403–16.
[12] McGuire RK. Probabilistic seismic hazard analysis and design earthquakes: closing the loop. Bulletin of the Seismological Society of America 1995;85(5):1275–84.
[13] Jayaram N, Lin T, Baker JW. A computationally efficient ground-motion selection algorithm for matching a target response spectrum mean and variance. Earthquake Spectra 2011;27(3):797–815.
[14] Baker JW, Lin T, Shahi SK, Jayaram N. New ground motion selection procedures and selected motions for the PEER transportation research

program. PEER 2011/03, Pacific Earthquake Engineering Research Center, University of California at Berkeley, 2011:80 pp.
[15] Wang G. A ground motion selection and modification method capturing response spectrum characteristics and variability of scenario earthquakes. Soil Dynamics and Earthquake Engineering 2011;31(4):611–25.
[16] Boulanger RW, Curras CJ, Kutter BL, Wilson DW, Abghari A. Seismic soil-pile-structure interaction experiments and analysis. Journal of Geotechnical and Geoenvironmental Engineering, ASCE 1999;125(9):750–9.
[17] Kramer SL, Arduino P, Shin HS. Using OpenSees for performance-based evaluation of bridges on liquefiable soils. PEER 2008/07. Pacific Earthquake Engineering Research Center, University of California at Berkeley; 2008 198.
[18] Bazzurro P, Cornell CA. Disaggregation of Seismic Hazard. Bulletin of the Seismological Society of America 1999;89(2):501–20.
[19] Baker JW, Jayaram N. Correlation of spectral acceleration values from NGA ground motion models. Earthquake Spectra 2008;24(1):299–317.
[20] Bianchini M, Diotallevi P, Baker JW. Prediction of inelastic structural response using an average of spectral accelerations. 10th International Conference on Structural Safety and Reliability (ICOSSAR09), Osaka, Japan, 2009:8 pp.
[21] Golafshani AA, Ebrahimian H, Bagheri V, Holmas T. Assessment of offshore platforms under extreme waves by probabilistic incremental wave analysis. Journal of Constructional Steel Research 2011;67(5):759–69.
[22] Tabandeh SA. Reliability and probabilistic seismic assessment of fixed jacket type offshore platforms. M.Sc. Thesis, Sharif University of Technology, Iran, 2010.
[23] Benjamin JR, Cornell CA. Probability, Statistics and Decision for Civil Engineers. McGraw-Hill; 1970 684.
[24] Campbell KW, Bozorgnia Y, Campbell-Bozorgnia NGA. Horizontal ground motion model for PGA, PGV, PGD and 5% damped linear elastic response spectra. Earthquake Spectra 2008;24(1):139–71.
[25] Department of Engineering and Construction, Pars Oil and Gas Company (POGC), Data Center, (accessed 20 June 2011).
[26] Carbon D, Combes Ph, Secanell R, Proudhon B. Preliminary seismic hazard assessment for Balal offshore oil field platform site (Persian Gulf). GEO-TER, Report No. GTR/TFE/0202-164, 2002a.
[27] Carbon D, Combes Ph, Secanell R, Proudhon B. Preliminary seismic hazard assessment for Parak and Tombak Onshore LNG Site (South-East Iran). GEOTER, Report No. GTR/TFE/1201-158, Rev1, 2002b.
[28] Carbon D, Secanell R. First approximation of SLE and RIE response spectra for the South Pars offshore SPD 12 project. GEO-TER, Report No. GTR/TOT/0105-236, 2005.
[29] Petroleum Development & Engineering Company. South Pars Gas Field Development Phase-1, Design basis data – offshore facilities. PEDEC-739-74005, 1995.
[30] API RP-2A WSD. Recommended practice for planning, design and constructing fixed offshore platforms –Working Stress Design. API Recommended Practice 2A-WSD, 21th edn., Supplement 3, 2007.